Submitted to *JGR Atmospheres*, February 1999

Polar vortex dynamics during spring and fall diagnosed using ATMOS trace gas observations

G. L. Manney,[1] H. A. Michelsen,[2] M. L. Santee,[1] M. R. Gunson,[1] F. W. Irion,[1] A. E. Roche,[3] N. J. Livesey[1]

Abstract

Trace gases measured by the Atmospheric Trace Molecule Spectroscopy (ATMOS) instrument during the Mar/Apr 1992 (AT-1), Apr 1993 (AT-2), and Nov 1994 (AT-3) space-shuttle missions have been mapped into equivalent latitude/potential temperature (EqL/θ) coordinates. The asymmetry of the spring vortices results in coverage of subtropical to polar EqLs. EqL/θ fields of long-lived tracers in spring in both hemispheres show the net effect of strong descent at high EqL in the upper stratosphere with decreasing descent at lower altitudes throughout the winter, and evidence of greater descent at the edge of the lower stratospheric vortex than in the vortex center; these results are consistent with trajectory calculations examining the history of the air measured by ATMOS in the month prior to each mission. EqL/θ tracer fields and parcel histories indicate regions of strong mixing in the 1994 southern hemisphere (SH) spring vortex above 500 K, with the strongest mixing confined to the vortex edge region between 500 and 700 K, and mixing throughout the northern hemisphere (NH) spring vortex in 1993 below about 850 K. Parcel histories indicate mixing of extravortex air with air near the vortex edge below 500 K in the SH, but not with air in the vortex core; they show extravortex air mixing well into the vortex above ~450 K in the NH, and into the vortex edge region below. The effects of denitrification, dehydration, and ozone depletion are apparent in EqL/θ HNO_3, H_2O, and O_3 in the SH lower stratospheric spring vortex, and ozone depletion is apparent in the NH spring. The morphology of HNO_3 in the Arctic spring lower stratospheric vortex is consistent with the effects of descent. Examination of H_2O+2CH_4 shows that dehydration in the SH extended up to ~600 K and suggests the possibility of a small amount of dehydration in the NH vortex below ~465 K. EqL/θ fields of ATMOS NO_y-NO_y^* (NO_y^* is the expected NO_y calculated from a prescribed relationship with N_2O for fall) show decreases consistent with the effects of mixing throughout the NH lower stratospheric vortex and along the vortex edge and above 600 K in the SH. The HNO_3 field, and the consistency of NO_y-NO_y^* with mixing, indicates that there was not significant denitrification during the 1992-93 NH winter. Differences in EqL/θ tracer fields during fall between the missions reflect the fact that each succeeding mission took place approximately 2 weeks later in the season; there was greater average descent of the air in the developing vortex during each succeeding mission, consistent with larger downward excursions of long-lived tracer contours in the upper stratosphere at high EqL. Trajectory calculations indicate greater isolation of proto-vortex air in later missions. Air originating in the tropics in the month preceding the AT-1 and AT-3 missions was sampled in the proto-vortex edge region; during AT-2 the proto-vortex was more quiescent and no tropical air was sampled.

polar processes
transport

1. Introduction

The space shuttle-borne Atmospheric Trace Molecule Spectroscopy (ATMOS) instrument is a high resolution Fourier transform infrared spectrometer that operates in solar occultation mode and simultaneously measures vertical profiles of approximately 30 species. During the three Atmospheric Laboratory for Applications and Science (ATLAS) missions in March/April 1992 (AT-1), April 1993 (AT-2), and November 1994 (AT-3) ATMOS observed middle and low latitudes during two austral (AT-1 and AT-2) and one boreal (AT-3) autumn, and high latitudes in and around the decaying polar vortex in one austral (AT-3) and one boreal (AT-2) spring, as well as the tropics during AT-1 and AT-3

[1]Jet Propulsion Laboratory/California Institute of Technology, Pasadena, California.
[2]Atmospheric and Environmental Research, Inc, San Ramon, California.
[3]Lockheed Martin Advanced Technology Center, Palo Alto, California.

[*Gunson et al.*, 1996].

Several studies have explored vortex versus extravortex conditions in spring using AT-2 and/or AT-3 ATMOS sunrise data. Although both AT-2 and AT-3 sunrise observations were taken in a narrow latitude band at high latitudes, since the polar vortex is strongly distorted and air is frequently drawn up from low latitudes in spring, these observations sample both vortex and extravortex air [e.g., *Manney et al.*, 1996b]. This is apparent in cross-sections as a function of longitude and potential temperature of ATMOS observations shown by *Abrams et al.* [1996a, c] and *Rinsland et al.* [1996a, b, 1999]. *Abrams et al.* [1996a, c] used long-lived tracer observations inside and outside the Antarctic and Arctic polar vortices to quantitatively estimate net descent over the winter. *Rinsland et al.* [1995, 1996a, 1999] compared vortex and extravortex ATMOS observations to study chlorine species, denitrification, and dehydration in the polar vortices.

Michelsen et al. [1998a] used N_2O and CH_4 data from the three ATLAS missions to show that there existed tight but distinct correlations between the two tracers in the tropics, the springtime vortex, and the extravortex/extra-tropics regions. The existence of distinct compact correlation curves can be useful in diagnosing mixing between air masses across "transport barriers" (such as the polar vortex) when those curves are nonlinear in the region between the two air masses of interest [*Waugh et al.*, 1997]. *Michelsen et al.* [1998b] used correlations of N_2O with NO_y and O_3 and estimates of mixing from N_2O and CH_4 to quantitatively estimate denitrification and chemical ozone loss in the Arctic and Antarctic spring vortices.

It has also been shown that, although the fall measurements from the ATLAS missions only extended up to about 50° latitude [*Gunson et al.*, 1996], the developing polar vortex (the "proto-vortex") was sufficiently asymmetric and variable [e.g., *Manney et al.*, 1996b] that air from within it was sampled, and tracer correlations for this air are distinct from those for midlatitude air [*Michelsen et al.*, 1998b]. *Michelsen et al.* [1998b] also provided polynomial fits to the ATMOS correlations of CH_4, NO_y, and O_3 with N_2O, for the various regions studied; the departure of the data from these relationships is useful in diagnosing regions where mixing and/or chemical processes are important.

Although it has been demonstrated that ATMOS data from the ATLAS missions sampled a variety of conditions despite limited spatial and temporal coverage, the full extent of the coverage of meteorological conditions was not realized in previous studies, since the observations were grouped in a few relatively broad categories (e.g., vortex and extravortex, or tropics and midlatitudes). Longitudinal cross-sections shown by *Abrams et al.* [1996a, c] and *Rinsland et al.* [1996a, b, 1999], while showing the dramatic changes demarking the vortex boundary, do not give a clear picture of the relative position of observations away from the vortex edge, and even blur the vortex boundary to some extent, since the position of the vortex changes during the missions.

A tool that has been commonly used in recent years for diagnosing the effects of dynamical and chemical processes in trace gas data is to display them on isentropic (constant potential temperature, θ) surfaces (along which air moves in absence of diabatic effects) as a function of potential vorticity (PV) [e.g., *Schoeberl et al.*, 1989, 1992; *Manney et al.*, 1994b] or equivalent latitude (the latitude that would enclose the same area as the corresponding PV contour) [e.g., *Butchart and Remsberg*, 1986; *Schoeberl et al.*, 1995; *Lary et al.*, 1995; *Manney et al.*, 1997; *Morrey and Harwood*, 1998; *Randel et al.*, 1998]. As well as showing trace gas distributions with respect to the underlying meteorological conditions, such fields are frequently useful for model initialization [e.g., *Lary et al.*, 1995; *Manney et al.*, 1998].

In the following, we present an overview of ATMOS observations from the three ATLAS missions mapped into equivalent latitude (EqL)/θ space. We focus on long-lived tracers (e.g., N_2O and CH_4) whose distributions provide information on transport and mixing processes; distributions of other species (e.g., O_3 and HNO_3) that have good "condition-space" coverage, and derived quantities that are useful in diagnosing mixing and/or chemical processes, are also shown. To aid in interpretation of these results, we also show air parcel histories obtained by running a large number of back trajectory calculations from the locations of the ATMOS observations. The results presented here provide information on the details and spatial effects of transport and mixing processes and the interplay between those processes and polar vortex chemistry in the lower stratosphere. They also provide a meteorologically-based context for comparison of the springtime Arctic and Antarctic vortices and of vortex development in fall.

2. Meteorological Conditions During the ATLAS Missions

The ATMOS data cover 25 Mar–2 Apr 1992 (AT-1), 8–16 Apr 1993 (AT-2), and 3–12 Nov 1994 (AT-3). Table 1 summarizes the spatial coverage of the Version 2 data used here; the coverage is shown in more detail by *Gunson et al.* [1996]. AT-3 and AT-2 sunrise observations were made at high latitudes in the southern hemisphere (SH) and northern hemisphere (NH) spring, respectively; AT-1 sunrise observations were in the tropics. Sunset observations from all three missions were in the fall when the polar vortex was developing, in the NH during AT-3 and in the SH during AT-2 and

Table 1. ATMOS Coverage during the ATLAS Missions

mission (dates)	sunrise/ sunset	seasonal conditions	latitude coverage	number of profiles	longitude distribution
AT–3	SR	spring	72.4°S–64.5°S	81	~uniform
(3-12 Nov 1994)	SS	fall	3.4°N–49.2°N	96	~uniform
AT–2	SR	spring	63.5°N–69.1°N	61	~uniform
(8-16 Apr 1993)	SS	fall	50.2°S–27.0°S	34	sparse ~ 60° to 180°E
AT–1	SR	tropics	28.2°S–30.5°N	45	sparse ~ -60° to 80°E
(25 Mar-2 Apr 1992)	SS	fall	55.5°S–21.9°S	39	none ~ -180° to -110°E

AT-1.

Meteorological data (temperature,geopotential height, horizontal wind) from the UK Meteorological Office (UKMO) troposphere-stratosphere data assimilation system [*Swinbank and O'Neill*, 1994] were used to calculate PV and "scaled PV" and analyzed to provide a meteorological context for the ATMOS observations. Scaled PV (sPV) is in "vorticity units" [*Dunkerton and Delisi*, 1986], as described by *Manney et al.* [1994c]. The UKMO data are provided on the Upper Atmosphere Research Satellite (UARS) standard pressure levels (6 levels per decade in pressure or about 2.5 km vertical spacing) extending up to 0.316 hPa (~2300–2500 K), but are not considered as reliable in the top few levels. Reliable and complete PV fields can thus be calculated up to about 2000 K. PV and sPV calculated from the UKMO data were interpolated (bilinearly in the horizontal and linearly in log(pressure) in the vertical) to the ATMOS observation locations and are provided with the Version 2 ATMOS data; this sPV will be used in Section 4 to grid the ATMOS data in EqL/θ space.

Plate 1 summarizes the meteorological conditions in the spring hemisphere during AT-3 and AT-2, showing |sPV| maps with temperature contours overlaid at representative levels in the middle and lower stratosphere, averaged over eight days during the AT-3 and AT-2 missions. The latitude bounds of the ATMOS observations are also indicated. The longitudinal position of the vortex remained sufficiently constant during each mission that these maps give a representative picture (*Manney et al.* [1996b] showed this for AT-3), although the extrema of PV values sampled are smoothed out. The vortex is demarked by a region of strong sPV gradients that occurs at different |sPV| values for varying dynamical situations. Comparison of the steepness of the sPV gradients between Plates 1a and b, or Plates 1c and d, gives an indication of the relative strength of the Antarctic and Arctic vortices at the levels shown. The Antarctic vortex is stronger throughout the winter than the Arctic vortex; it also breaks down later, especially in the lower stratosphere [e.g., *Manney et al.*, 1994c, and references therein]. Thus, the vortex was larger and stronger at both levels during AT-3 than during AT-2, although AT-3 was about two weeks later in the spring than AT-2.

The polar vortex in the SH typically breaks down starting at the top, and the erosion is relatively gradual; although tongues of material are drawn off of the vortex, they are not generally so large that an individual tongue represents a substantial portion of the vortex [e.g., *Manney et al.*, 1994c]. As these tongues are drawn out, air is also drawn in around the vortex edge from low latitudes, with $|\mathrm{sPV}| \lesssim 0.6 \times 10^{-4}$ s^{-1} (subtropical values) observed at the latitudes sampled by ATMOS. Plate 1a shows that during AT-3 there was still a relatively strong (although weaker and smaller than in midwinter) vortex in the SH middle stratosphere; *Manney et al.* [1996b] and *Abrams et al.* [1996a] showed that well-defined vortex remnants were present at levels up to ~1300 K during this mission.

As seen in Plate 1b, the situation in the Arctic middle stratosphere is more complicated. The Arctic vortex was in the midst of breaking down in a more rapid and dramatic manner than in the SH. At the beginning of AT-2, a huge tongue of vortex air had been drawn out, representing a significant fraction of the vortex area. As the mission progressed, this tongue of vortex air was drawn further out, and, starting about 13 Apr 1993, wrapped back upon itself around the anticyclone over the pole, so that a cross-section of the hemisphere from 90° to 270°E over the pole would have sampled vortex air in three places: in the main vortex remnant along 90°E at ~60-80°N, in the tail of the drawn-out tongue over the pole, and in the main part of the tongue along 270°E at ~30-50°N. Low-PV air was drawn up between the vortex and the tongue into the anticyclone and coiled up with the tongue of vortex air. Thus, on indi-

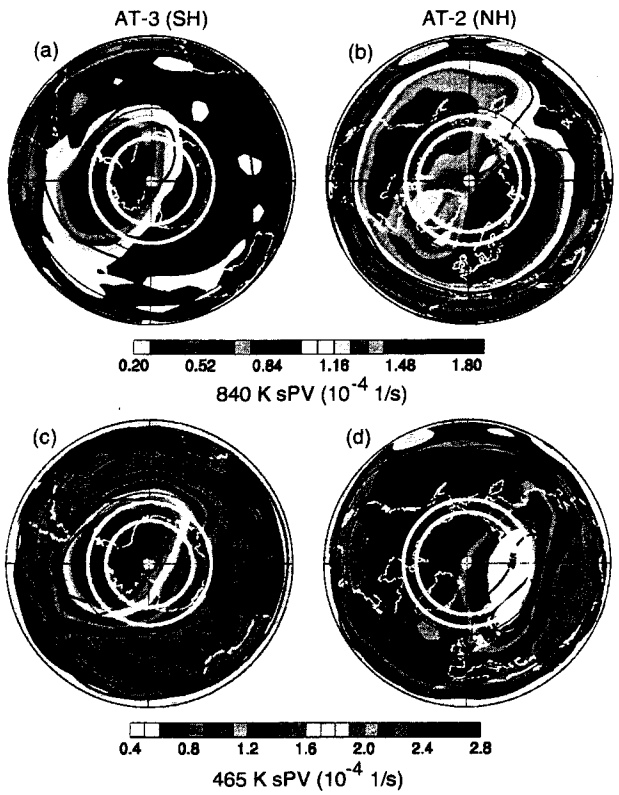

Plate 1. Maps of the absolute value of scaled potential vorticity (|sPV|) on the 840 K (a and b) and 465 K (c and d) isentropic (potential temperature, θ) surfaces, averaged over 4-11 Nov 1994 during AT-3 (a and c), and 8-15 Apr 1993 during AT-2 (b and d), in the spring hemisphere (southern hemisphere (SH) for AT-3, northern hemisphere (NH) for AT-2). Absolute value is shown since sPV decreases (to higher negative values) toward the pole in the SH. Overlaid in black are temperature contours of 230, 240, and 250 K at 840 K (a and b) and 205, 210, and 215 K at 465 K (c and d). The thick white circles show the bounds of the latitude coverage during the AT-3 (a and c) and AT-2 (b and d) missions. The map projection is orthographic, with 0° longitude at the bottom in the NH maps and at the top in the SH maps, and 90°E to the right. The domain is from equator to pole, with thin dashed lines at 30° and 60° latitude.

vidual days, ATMOS could have sampled vortex air in two or three separate places, as well as midlatitude air (sPV $\lesssim$ 0.9×10^{-4} s^{-1}). The average in Plate 1b shows a broader tongue and higher sPV values between the main vortex and the tongue than on the individual days, as the shape and position of the tongue changed significantly during the mission. This tongue extended from ~700–1100 K. Above that level, the polar vortex had already dissipated. The large tongue of vortex air resulted in a temporary increase in the area enclosed by the moderately high sPV contours inside the vortex edge, while the area enclosed by the highest sPV contours in the vortex core was small and shrank during AT-2.

Interhemispheric differences in meteorological conditions in the middle stratosphere were also reflected in the temperatures. During AT-3, a summer-like temperature pattern was already present in the middle and upper stratosphere, with high temperatures centered over the pole. In contrast, during AT-2 the Arctic middle stratosphere had not completed this transition, and temperatures at 840 K were nearly constant, with slightly higher temperatures appearing at high latitudes.

In the lower stratosphere, the SH vortex during AT-3 was still strong and only slightly smaller than its midwinter dimensions [*Manney et al.*, 1996b]; the Antarctic lower stratospheric vortex typically remains intact into December [*Manney et al.*, 1994c]. In contrast, the NH lower stratospheric vortex during AT-2 was much smaller than in midwinter, but still defined by strong PV gradients. The Arctic lower stratospheric vortex during the 1992-93 winter was the strongest on record, with maximum PV gradients approaching values typical in Antarctic winter [*Manney et al.*, 1994a; *Zurek et al.*, 1996]; *Manney et al.* [1994a] and *Dahlberg and Bowman* [1995] showed that this led to substantially less exchange across the vortex edge than is usual in the Arctic. Note also that the lower stratospheric vortex (defined by the region of strong PV gradients) was delimited by higher |sPV| values in the NH than in the SH: |sPV| values around 1×10^{-4} s^{-1} were representative of the vortex edge in the austral lower stratosphere, but represented midlatitude conditions in the boreal lower stratosphere. This is consistent with the NH final warming being more advanced, since the region of strong PV gradients typically shifts to higher PV values as the vortex erodes [e.g., *Manney et al.*, 1994a; *Waugh and Randel*, 1999]. In both hemispheres the lower stratospheric vortices were eroded mainly via small filaments drawn off the vortex and stretched out into midlatitudes where they eventually mixed down to ambient conditions; *Newman et al.* [1996] and *Waugh et al.* [1997] showed that some such vortex fragments were still present in May 1993 in the Arctic. Consistent with the colder winter and later final warming in the SH, minimum high latitude temperatures at 465 K were about 6–8 K lower during AT-3 than

during AT-2.

At both representative levels shown in Plate 1, AT-3 and AT-2 provided good coverage of the vortex, including observations in the vortex core. During AT-3, air from sufficiently low latitudes was drawn up around the vortex that AT-3 sampled subtropical air. During AT-2, since the ATMOS observations covered a narrower latitude band, and less air was being drawn in from low latitudes, little subtropical air was sampled.

In fall there is less interhemispheric [e.g., *Manney and Zurek*, 1993] and, in both hemispheres, less interannual [e.g., *O'Neill and Pope*, 1990] variability in dynamical processes than in winter or spring. Meteorological conditions in the fall hemisphere during each of the ATLAS missions are summarized in Plate 2. The major difference between conditions during each of the ATLAS missions was the greater development of the vortex in each succeeding mission as the observations were taken about two weeks later in the season in AT-2 than AT-1, and a further two weeks later in AT-3 than in AT-2. The fall polar vortices develop from the top down [e.g., *Waugh and Randel*, 1999], as is evident in the much greater development of the proto-vortex at 1100 K than at 520 K. *Manney et al.* [1996b] showed that the proto-vortex was evident at levels down to ~450 K during AT-3; a significant region of strong PV gradients extends only down to ~500 K during AT-2. As seen in Plate 2f, during AT-1 there was only a very small region of enhanced PV gradients at 520 K. The temperatures also reflect the further development of the fall vortex during each succeeding mission, especially at 520 K where the temperatures were dropping rapidly at this time.

The proto-vortices in the middle and upper stratosphere during AT-1 and AT-3 were both distorted and shifted off the pole (Plate 2a,c). In contrast, the proto-vortex during AT-2 (Plate 2b) was on average symmetrical and pole-centered. During all three missions, however, maps for individual days show that the proto-vortex wobbled about, and tongues of air were drawn off the vortex edge. During AT-3, the vortex was preferentially shifted towards the Greenwich meridian, as is typically the case later in the Arctic winter when the "Aleutian high" has formed [e.g., *Juckes and O'Neill*, 1988], and tongues of air were pulled off near ~250°E and drawn out to ~30°N. During AT-2 the vortex shape and position were more variable (hence the symmetric average), and smaller tongues of material were pulled off the edge at several locations on different days. During 12–14 Apr 1993 (AT-2), the proto-vortex extended towards the dateline, and a tongue of material drawn off the vortex edge near ~150°E was pulled out to nearly 30°N. During AT-1, the proto-vortex area was smaller and, although material can be seen drawn off the edge, these events were smaller, shorter-lived, and did not in general transport proto-vortex air to as low latitudes as those seen in AT-2 and AT-3. The situation in the lower stratosphere during the three missions was roughly similar to that at the higher levels, except that the vortex was just beginning to develop and thus PV gradients were still much weaker than winter values, and, especially during AT-1, did not yet represent a substantial transport barrier.

Although the ATMOS observations extended up to only ~50° in the fall hemisphere (Table 1), the variability described above, and proto-vortex material extruded to low latitudes, enabled ATMOS to sample proto-vortex air during each mission. The sampling was better in AT-3 than AT-2 or AT-1, due to the greater development of the vortex; although the vortex was more developed during AT-2 than AT-1, the sampling range was very limited (Plate 2).

Because of the variability and asymmetry of the vortex, the ATMOS observations taken in limited latitude bands cover a wide variety of meteorological conditions. By viewing these observations from a vortex-centered perspective, we can examine how the meteorological conditions shaped the detailed structure of the trace gas fields measured by ATMOS using a physically-based context for comparison between the missions.

3. Data and Analysis

3.1. ATMOS Data

The horizontal coverage of the ATMOS data was summarized in Table 1 (Section 2). The ATMOS Version 2 data cover altitudes ranging from 12 to 80 km with a vertical resolution of 2–3 km [e.g., *Abrams et al.*, 1996b]. For each occultation, the signal-to-noise ratio was enhanced by the use of one of a set of six optical bandpass filters (numbered 1, 2, 3, 4, 9, and 12; some filters were not used in all missions). N_2O was measured with all six filters, CH_4, O_3, and HNO_3 were measured in five filters, H_2O in four, and other trace gases in three or fewer. *Gunson et al.* [1996] summarize the altitude coverage, filters used, and estimated precision for each species, in addition to showing the spatial coverage during each mission.

A summary of some critical features of the processing methodology and discussion of the error budget for the Version 2 ATMOS data are given by *Abrams et al.* [1996b]. The experimental uncertainties vary with species, filter, and altitude. O_3, N_2O, CH_4, and HNO_3 typically have precision better than 5%, H_2O and NO_2 typically better than 10%, NO and N_2O_5 typically better than 20%, and $ClONO_2$ and HNO_4 worse than 20%. Data from filter 4 show a large systematic bias in the Version 2 retrievals below about 25 km; we do not use filter 4 data below 30 km. Data from filter

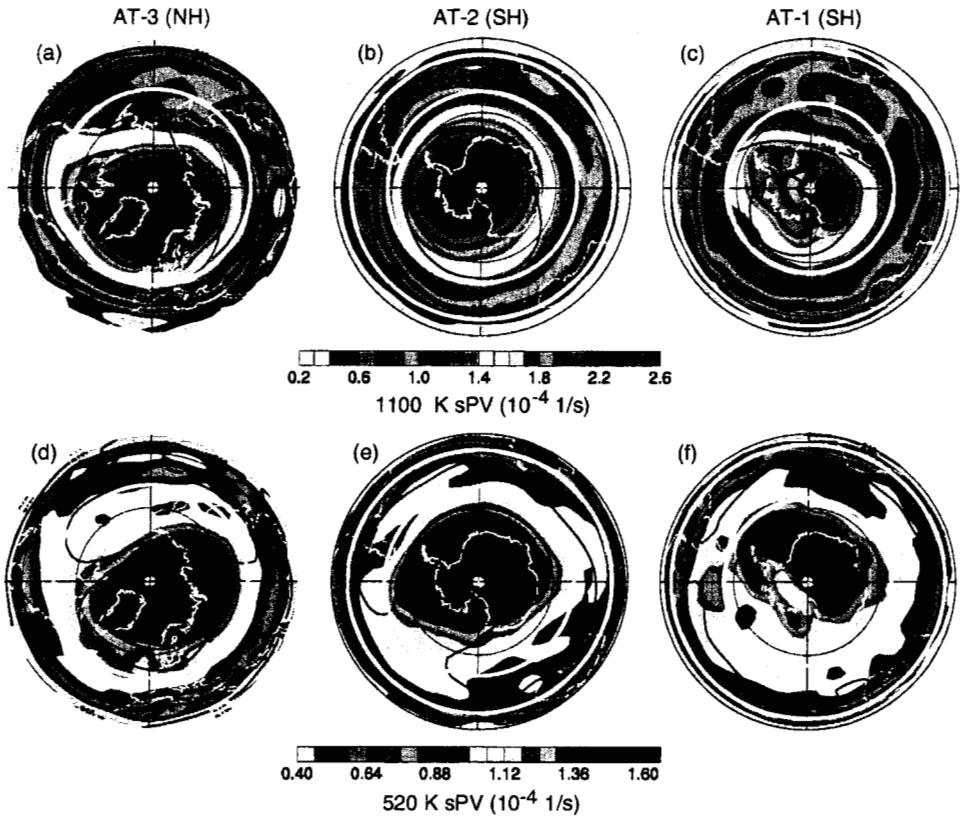

Plate 2. |sPV| maps on the 1100 K (a, b, and c) and 520 K (d, e, and f) isentropic surfaces, averaged over 4–11 Nov 1994 during AT-3 (a and c), 8–15 Apr 1993 during AT-2 (b and e), and 25 Mar–1 Apr 1992 during AT-1 (c and f) in the fall hemisphere (NH for AT-3, SH for AT-2 and AT-1). Overlaid in black are temperature contours of 220, 230, and 240 K at 1100 K (a, b and c) and 205, 210, and 215 K at 520 K (d, e and f). The thick white circles show the bounds of the latitude coverage during the AT-3 (a and d, the low latitude circle is along the edge of the plot), AT-2 (b and e), and AT-1 (c and f) missions. The layout is as in Plate 1, except different θ levels are shown.

12 are excluded below 20 km because of a systematic bias. The estimated retrieval uncertainties are used for weighting in the gridding procedure, as described in Section 3.2.

At the top and bottom altitudes of the measurement range, the ATMOS Version 2 data occasionally include some unphysical values that are not accompanied by large uncertainties. In order to detect and remove the worst of these, the tops and bottoms of the profiles were checked for unphysically large gradients and negative mixing ratios before gridding, and a few points from some profiles were excluded on this basis. These "quality-control" criteria were adjusted so as to exclude most of the values identified as unrealistic, but to include all values that could be physically-based. The number of data points excluded is small, typically 0-10 for a given species and mission.

3.2. Equivalent-latitude/θ Mapping of ATMOS data

To grid the ATMOS observations in PV/θ-space, we take a weighted average of all observations falling within a prescribed distance in PV and logθ of the desired gridpoint. As well as being weighted by distance, the values averaged at each gridpoint are weighted by the estimated retrieval uncertainty using the same function as for the spatial weighting, with the error half-width and cutoff determined by the expected precision for each species [*Abrams et al.*, 1996b]. A number of combinations of weighting parameters were tested and compared with simple unweighted averages of binned data. The gridding is not particularly sensitive to the weighting function; a Gaussian was used in the plots shown below. The half-width in θ was selected so as to make the vertical spacing approximately 2 km, comparable to the vertical resolution of the ATMOS data. The selection of half-width for the weighting function in PV is more problematic, and is based on striking a balance between a reasonable number of gridpoints in regions where PV gradients are weak (which argues for closer spacing) and not too many empty gridboxes in regions where there is good data coverage, but PV gradients are very strong. This is particularly problematic during AT-3, when there were extremely strong PV gradients around the vortex in the austral lower stratosphere, and extremely weak PV gradients in the austral upper stratosphere [*Manney et al.*, 1996b].

The PV half-widths (ΔsPV) selected are 0.2×10^{-4} s^{-1} for AT-3, and 0.15×10^{-4} s^{-1} for AT-1 and AT-2. For N_2O (a species that is measured in all six filters) these values give ~1–40 points in each non-empty grid box for AT-3, ~1-30 for AT-2, and ~1-20 for AT-1. The gridding routine then uses all data within two half-widths in PV and θ of the gridpoint in the average; however, a value is not calculated unless there is at least one observation within one half-width of the gridpoint. The error weighting allows inclusion of any data with uncertainty less than 100%.

For derived products combining several species measured by ATMOS (e.g., NO_y), each species is first individually gridded in PV/θ space, and then the species are combined after gridding. This method allows combination of species that were not measured simultaneously (i.e., in the same filters), but measured under the same meteorological conditions, and thus provides the fullest coverage for the derived products. For calculations of NO_y, profiles of the species used are extrapolated above and below the measurement range as described by [*Rinsland et al.*, 1996a], except that HNO_3 is not extrapolated at the bottom and NO is not extrapolated at the top. Thus, NO_y is calculated only where ATMOS observed HNO_3 in the lower stratosphere (where it constitutes the bulk of NO_y) and where ATMOS observed NO in the upper stratosphere.

After gridding in PV/θ space, EqL is calculated for each PV gridpoint value, and the fields are interpolated linearly to a uniform EqL grid. The interpolation routine is restricted from filling across large gaps; thus, the coverage in the plots shown below is representative of the actual coverage of the ATMOS observations.

3.3. Parcel History Calculations

We use back trajectory calculations to examine the recent history of air at the locations of the ATMOS observations. The trajectory code is described by *Manney et al.* [1994c]; it is in isentropic coordinates and includes a calculation of diabatic descent to obtain vertical velocities in that coordinate system. The UKMO horizontal winds are used, and UKMO temperatures are used in the radiation calculation to estimate vertical velocities.

The initial parcel positions were determined in a manner similar to that described by *Manney et al.* [1998]. At the location (latitude and longitude) of each ATMOS observation, a column of parcels was initialized on 100 isentropic surfaces equally spaced in logθ between 380 and 2000 K (this is the same vertical range for which the EqL/θ space plots of ATMOS data are constructed). On each surface, 121 parcels were initialized in a 1° by 1° box centered at the ATMOS measurement location, giving 12,100 total parcels for each ATMOS profile. Back trajectory calculations were run for 32 days, each started from the time (closest 1/2 hour, the trajectory time step) of the corresponding ATMOS observation; the parcels positions were saved every four days. These calculations were designed to be used for several purposes. For short time periods (~4–12 days) they can be used to reconstruct high-resolution tracer profiles, as done by *Manney et al.* [1998], to examine the origins of details of the profile structure [*Manney et al., in preparation*].

For the approximately month-long duration of the runs, the positions of individual parcels are, of course, uncertain, due to accumulated errors from a number of sources, one of the largest being inaccuracies in the advecting winds [e.g., *Morris et al.*, 1995]. However, much useful information can be obtained from three-dimensional trajectory calculations of this length, provided a reasonably large number of parcels are averaged. For example, *Manney et al.* [1997, and references therein] successfully computed vortex-averaged trace gas values using 30- to 40-day trajectory-based transport calculations. Trajectory calculations of several months' duration have frequently been used to examine general features of air motion [e.g., *Fisher et al.*, 1993; *Manney et al.*, 1994c]. A very large number of parcels was used here (~2.1 million for AT-3, 1.1 million for AT-2, and 1.0 million for AT-1) to facilitate averaging over various domains.

Results from the trajectory calculations are displayed by mapping the historical characteristics of the parcels into EqL/θ space in the same manner as for the ATMOS data. That is, the positions of the parcels (e.g., latitude, Δθ, sPV) at the end of the back trajectory run, or data (e.g., idealized trace gas fields) interpolated to those positions, are taken as the field to be gridded, with the gridding coordinates being the initial positions (PV, θ) at the ATMOS observation locations. This produces a map of the characteristics 32 days earlier of the air sampled by ATMOS. If the same PV/θ grid is used as for the ATMOS data, there are ~50 to several thousand parcels in each gridbox, providing reasonable statistics for averaging. The gridding procedure is the same as described above for the ATMOS data, except that no weighting for uncertainty is used. Because there are many parcels in each gridbox, the scatter in values within a box gives information on the homogeneity of the historical characteristics of air that ended up in a certain region sampled by ATMOS.

Besides examining vertical and horizontal motion and PV changes over the period, we have produced idealized transport calculations over the period for N_2O, CH_4, and H_2O by using idealized tracers derived from UARS Microwave Limb Sounder (MLS) or Cryogenic Limb Array Etalon Spectrometer (CLAES) data (Section 3.4) interpolated to the final parcel positions as the field to be gridded. This is an application of the reverse-trajectory procedure developed and described in detail by *Sutton et al.* [1994]. The UARS-based fields that are used for tracer initialization are very smooth, and we expect only large-scale qualitative agreement between these fields and ATMOS data; nevertheless, the qualitative changes in tracers resulting from transport calculations initialized in this way are useful in comparing the calculated large-scale tracer motion with that expected from the appearance of the ATMOS observations.

3.4. Ancillary Data

We use data from the UARS CLAES and MLS instruments to produce idealized tracer initialization fields and to illuminate certain aspects of the flow during the ATLAS missions. During all three ATLAS missions, the latitude coverage of the UARS observations used here was ~80°S to 30°N. Both CLAES and MLS were fully operational during AT-1 and AT-2; AT-3 occurred after CLAES had depleted its cryogen and the radiometer that measured H_2O on MLS had failed. MLS did, however, measure O_3, HNO_3, and ClO during most (5 through 11 Nov 1994) of AT-3.

For model initialization we have constructed a set of idealized tracer fields in EqL/θ space from CLAES N_2O and CH_4 and MLS H_2O. Since UARS switches 10 times a year between viewing high northern and high southern latitudes (yaws), in order to get global fields, we average (in EqL/θ space) the data from three days with complete coverage on either side of the yaw day. Data from late April 1992 through early April 1993 were used to produce 10 such files for each species (one for each "UARS month"), each of which is assigned to the day of year in the middle of the averaging period. To reconstruct a field for use in initialization for a particular day, the PV for that day is used with an EqL/θ field of the tracer that is linearly interpolated in time between the nominal dates of the two neighboring standard EqL/θ fields. The data used to produce the files for this "climatology" are Version 8 CLAES N_2O, Version 7 CLAES CH_4, and MLS H_2O from the prototype nonlinear retrievals described by *Pumphrey* [1998]. Version 7 CLAES N_2O and CH_4 validation is discussed by *Roche et al.* [1996]; Version 8 CH_4 was not used because it showed an even stronger high bias than Version 7 when compared to correlative data.

We also show some MLS O_3 data taken during AT-3; these are preliminary Version 5 data. The MLS Version 3 O_3 data validation was discussed by *Froidevaux et al.* [1996]; some Version 3/Version 4 differences are noted by *Manney et al.* [1996a]. Version 5 data have higher vertical resolution than the previous versions (6 surfaces per decade in pressure as opposed to 3). Previous biases (~1 ppmv) in the MLS lower stratospheric O_3 data, as compared to SAGE II and other correlative sources, have been significantly reduced in the Version 5 data; differences between Version 4 and 5 in the middle and upper stratosphere are small.

Detailed comparisons of ATMOS with UARS CLAES, MLS, and Halogen Occultation Experiment (HALOE) trace gas data have been done in EqL/θ space. These intercomparisons show very good overall agreement between the morphology of the tracer fields and indicators of transport, despite some biases between the data sets [*Manney et al., in preparation*].

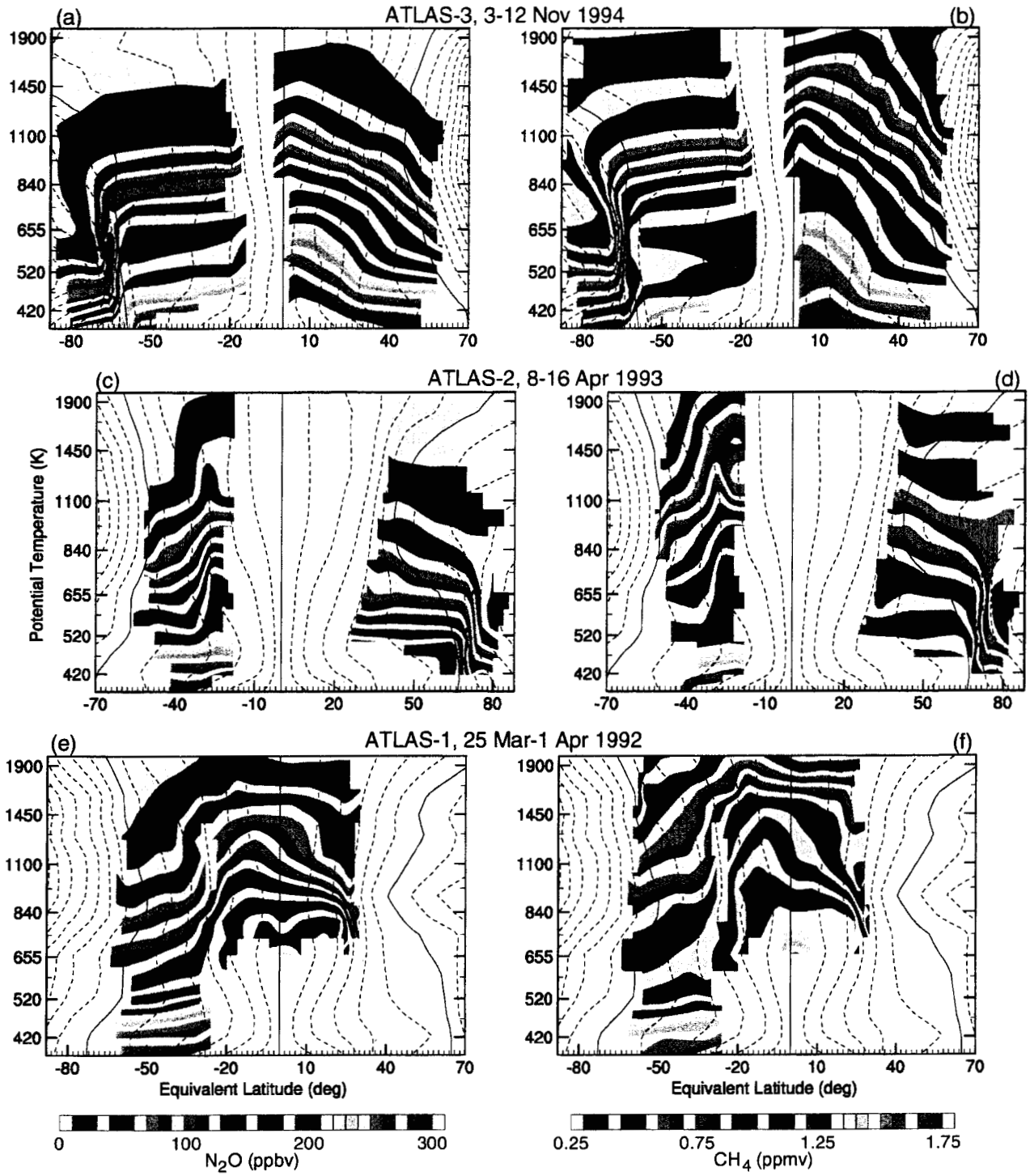

Plate 3. Equivalent Latitude (EqL)/θ space fields of ATMOS N_2O (left) and CH_4 (right) from AT-3 (a and b), AT-2 (c and d), and AT-1 (e and f). The vertical range is from 380 to 2000 K. AT-3 and AT-1 fields are shown from 88°S to 70°N; AT-2 fields are shown from 70°S to 88°N. The thin black lines are contours of |sPV|, averaged over 4–11 Nov 1994 for AT-3, 8–15 Apr 1993 for AT-2, and 25 Mar–1 Apr 1992 for AT-1 (the same days shown in Plates 1 and 2; days at the beginning and end of the ATLAS missions with only one or two ATMOS observations are excluded); the contour interval is 0.2×10^{-4} s^{-1}, with the 1.2×10^{-4} s^{-1} contour (typically in the vortex edge region) represented by a solid line, and the rest dashed lines; the smallest contour is 0.2×10^{-4} s^{-1}, on either side of the vertical line representing 0° EqL, with values increasing towards the poles. Note that for AT-2 and AT-1, the sPV contour interval shown here is *not* the same as the interval used for gridding (Section 3.2).

4. Results

4.1. ATMOS Trace Gas Fields

Plate 3 shows EqL/θ space maps of ATMOS N_2O and CH_4 observations from the ATLAS missions. The overlaid |sPV| contours indicate the position and strength of the polar vortex. N_2O and CH_4 are both long-lived in the stratosphere and are thus good tracers of air motions.

The mapping of AT-3 and AT-2 sunrise observations, in the Antarctic and Arctic spring vortices, respectively, demonstrates dramatically how fully the ambient conditions can be covered with observations taken in a very narrow latitude band (approximately 8° and 6° wide for AT-3 and AT-2, respectively). As shown above (Plate 1) for a representative level, subtropical air was drawn into the region of ATMOS observations throughout the AT-3 mission, over most of the depth of the stratosphere. As a result, AT-3 covered subtropical conditions everywhere except in the lowest part of the stratosphere (below ~450 K), where motions are dominated by smaller scales, and large tongues of air are not commonly transported as far from their origins. Although the final warming had progressed further during AT-2 than during AT-3, and no large tongues of subtropical air were sampled, the variability was still large enough that AT-2 had good coverage of midlatitude conditions through most of the stratosphere. The gain in coverage over the latitudes sampled is more modest for the sunset observations in fall, but the proto-vortex is sufficiently variable that the measurements typically reach ~60° EqL, along the inside of the proto-vortex edge.

A number of previously noted features of tracer transport in relation to the polar vortex are apparent in the ATMOS N_2O and CH_4 fields. *Abrams et al.* [1996a, c] used ATMOS N_2O and CH_4 profiles inside the vortex to estimate net winter descent for the SH using AT-3 data and for the NH using AT-2 data. The effects of this descent are apparent in Plate 3, with much lower vortex than extravortex values of the tracers at all levels below about 1000 K (where air is still relatively confined within the vortex). CH_4 values typical of the lower mesosphere ($\lesssim$0.3 ppmv) were seen at levels from ~650 to 840 K (~25–30 km) during AT-3, consistent with the results of *Abrams et al.* [1996a], and values typical of the upper stratosphere at levels from ~500 to 650 K during AT-2, consistent with *Abrams et al.* [1996c]. Other indications of the patterns of descent are more readily apparent than in previous results. The packing of tracer contours into the lower stratospheric vortex (i.e., extremely large vertical tracer gradients in the vortex interior) results from the patterns of descent over the winter, with strongest descent in the upper stratosphere, decreasing by more than an order of magnitude from the upper to the lower stratosphere [e.g., *Fisher et al.*, 1993; *Manney et al.*, 1994c]. Note that substantial horizontal tracer gradients are apparent across the vortex edge even at the lowest levels shown (down to 380 K in the SH). The apparent lack of contrast between vortex and extravortex values noted by *Abrams et al.* [1996a] was due in part to the saturation of their color palette and the packing of contours in the lower stratospheric vortex. The average vortex and extravortex profiles shown by *Abrams et al.* [1996a] converge below ~15 km, suggesting that the pattern of vortex confinement does not extend far below the lower limit of our plot (~16 km).

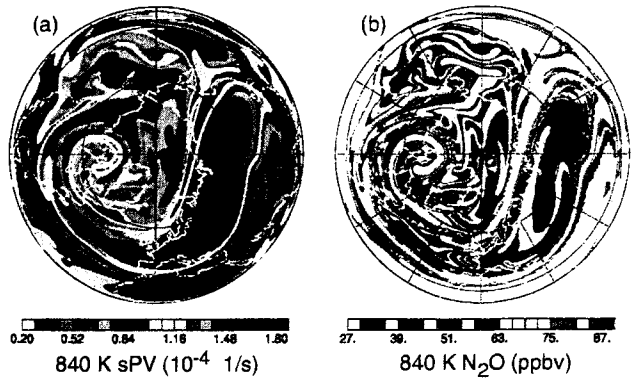

Plate 4. High resolution NH maps of sPV (a) and reconstructed N_2O (b) on the 840 K isentropic surface, on 16 Apr 1993, the last day of AT-2. The maps are constructed using reverse-trajectory calculations (Section 3.3). The map projection is orthographic, with 0° longitude at the bottom and 90°E to the right. The domain is from equator to pole, with thin dashed lines at 30 and 60°N.

An additional feature that was not previously apparent is the downward excursion of tracer contours along the vortex edge in the lower stratosphere (at the location of strongest sPV gradients), which is seen in both NH and SH spring. This observation suggests the results of greater descent along the vortex edge than in its center. Such a pattern is consistent with the results of *Manney et al.* [1994c], whose calculations showed largest descent rates in the lower stratosphere along the vortex edge throughout the winter in the SH, and during late winter/spring in the NH. This pattern is also reflected in N_2O/CH_4 correlations for AT-3, which show a larger difference between the vortex edge and midlatitude correlations than between the vortex interior and midlatitude correlations [*Michelsen et al., Maintenance of high HCl/Cl_y and NO_x/NO_y in the Antarctic vortex: A chemical test of confinement during Austral spring, submitted to J. Geophys. Res., Atmospheres*].

Above ~1100 K in the SH during AT-3 and ~800 K in

the NH during AT-2, strong tracer gradients are no longer apparent. The extremely large tongue of vortex material pulled out into midlatitudes during AT-2 between ~700–1100 K is reflected in the increase between those levels of the area covered by the PV contours. As noted in Section 2, this large tongue of material is coiled up with some low-latitude air in the anticyclone at latitudes sampled by ATMOS. Plate 4 shows 840 K maps of high resolution sPV from a reverse-trajectory calculation (Section 3.3) and high resolution N_2O reconstructed from this sPV field and the ATMOS EqL/θ space field shown in Plate 3c. The tongue of air that was pulled off the vortex underwent considerable mixing with low-latitude air pulled in around the vortex, and PV gradients in this region are much weaker than those at the same sPV values along the vortex edge. Thus, the sPV gradients seen in Plate 3c and d near 50° EqL are considerably weaker than those around the vortex edge, and the EqL/θ plot does not clearly indicate that there is a relatively strong and confined vortex remnant still present at these levels. Above ~1100 K the vortex has dissipated, and the tracer values are well-mixed combinations of former vortex and extravortex air.

As seen in Plates 3a and b, the region of minimum tracer mixing ratios in the vortex during AT-3 showed low values confined closer to the pole with increasing altitude, coinciding approximately with the decrease in the area enclosed by strong PV gradients. This decrease in area indicates that the vortex was severely eroded, and strong mixing was taking place: low vortex tracer values have been mixed with high extravortex values, resulting in the higher values at high latitudes at levels where the vortex was breaking down. Since N_2O and CH_4 have different vertical gradients, confined descent within the vortex results in different horizontal gradients along the vortex edge. This in turn results in dissimilar contour shapes for the two tracers in the vortex and along its edge, as quasi-isentropic mixing across the vortex edge affects them differently [e.g., *Strahan et al.*, 1996]. Thus, the regions near the lower stratospheric vortex where the N_2O and CH_4 contour shapes differ markedly (e.g., between ~600 and 800 K in the SH during AT-3) are regions of enhanced mixing of vortex and extravortex air. We will return to this point in Section 4.2.

More subtle variations in tracer morphology indicate differing dynamical conditions in the fall hemispheres during the three missions. In each succeeding mission, the contours are overall tilted more steeply down at high EqL, indicating the effects of more unmixed descent as the vortex develops. The increase in unmixed descent results from both an increase in the diabatic descent rates and, more importantly, a stronger transport barrier along the proto-vortex edge, so that the effects of descent are not diluted by mixing with air that has not experienced strong descent. Both effects are consistent with the later date of each succeeding mission. A distinct difference in the strength of the subtropical horizontal tracer gradients in the fall hemisphere, especially in the upper stratosphere, was seen between AT-1 and AT-3 (near 20 to 30° EqL); although AT-2 observations did not extend as far into the tropics, the tracer gradients from this mission appeared to be more similar to those during AT-1. Steeper subtropical gradients in the upper stratosphere during AT-1 and AT-2 than during AT-3 are consistent with those seen in zonal means of HALOE observations for similar time periods [*Ruth et al.*, 1997]. These differences likely result from the interplay between the seasonal cycle, the semiannual oscillation, and the quasi-biennial oscillation [e.g., *Ruth et al.*, 1997; *Randel et al.*, 1998].

ATMOS measured several other long-lived species, including HF, F11, F12, and SF_6 [*Gunson et al.*, 1996], as well as CO, which is long enough lived in some regions to use as a tracer of air motion [*Allen et al.*, 1999]. Since these species had either very limited vertical coverage or were measured in only one or two filters, their mapping in EqL/θ space is limited. However, during AT-3 there was enough coverage to indicate that these tracer observations showed a signature of unmixed descent within the vortex, i.e., a confined region of values typical of the upper stratosphere/lower mesosphere bounded by very strong gradients, and those with observations near the lower stratospheric vortex edge showed the downward excursion of contours indicative of enhanced descent.

Plate 5 shows similar plots of H_2O and HNO_3 observed by ATMOS. H_2O is a long-lived tracer in most of the extra-tropical stratosphere, with the exception of the Antarctic lower stratospheric vortex, where sedimentation of polar stratospheric clouds (PSCs) results in severe dehydration. HNO_3 builds up via chemical processes in the winter polar vortex [e.g., *Austin et al.*, 1986], with maximum mixing ratios near 25 km, and builds up in the lower stratospheric vortex via descent of these high values and production by heterogeneous chemical reactions linked to PSCs [*Santee et al.*, 1999, and references therein]; in the Antarctic, PSCs are prevalent for much of the winter, and sedimentation also leads to strong denitrification. Several studies have suggested that small amounts of dehydration and denitrification may occur in the Arctic vortex during especially cold winters [e.g., *Fahey et al.*, 1990b; *Vömel et al.*, 1997; *Hintsa et al.*, 1998].

The features described above in N_2O and CH_4 are also apparent in H_2O, including the signature of descent in the spring polar vortices during AT-2 and AT-3, evidence of mixing at levels where the vortex was decaying, and a successively steeper downward slope of the H_2O contours in the

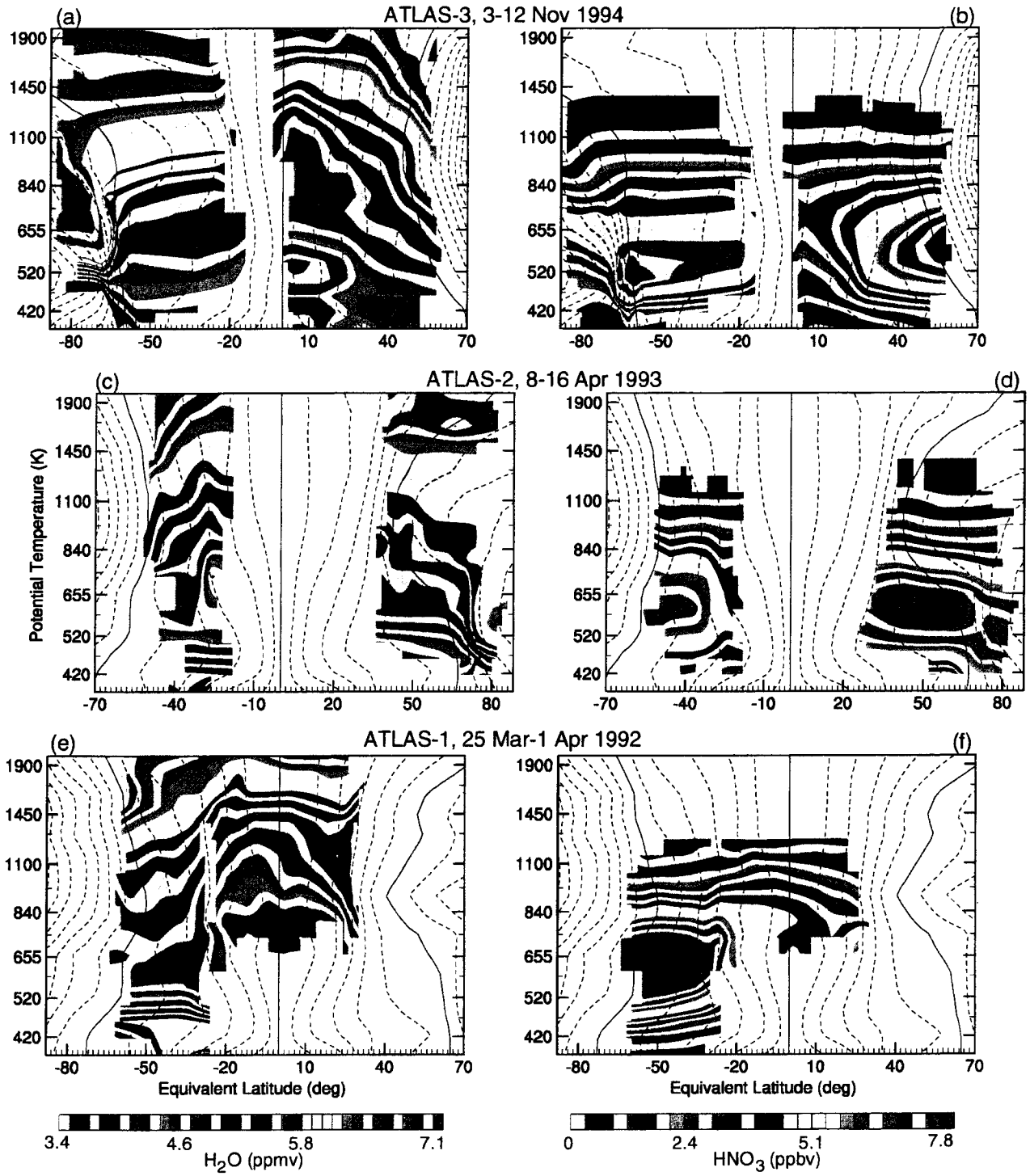

Plate 5. EqL/θ space fields of ATMOS H_2O (left) and HNO_3 (right). Layout is as in Plate 3.

fall hemisphere in each succeeding mission. Dehydration is apparent in the SH vortex up to at least ~500 K, as previously indicated by *Rinsland et al.* [1996a]; the highest dehydrated altitude cannot readily be deduced from this figure since the competing effect of descent of higher H_2O and the mimicking effect of mixing of lower extravortex H_2O (above ~500 K) must be considered. Although the interpretation is complicated by the dehydration, the H_2O distribution along the vortex edge in the lower stratosphere does show a downward tilt in the contours suggesting stronger descent along the vortex edge. This pattern is not apparent in the NH during AT-2, as it was in other tracers. However, since this feature was small and apparent only in the lowest levels shown in a region where there are only a few observations in each gridbox, the lack of such a feature in H_2O could reflect a sampling or data quality deficiency. Alternately, it may indicate a small amount of dehydration, which has previously been suggested to have occurred in the 1992-93 Arctic winter [*Michelsen et al.*, 1999].

Denitrification in the Antarctic vortex is apparent in the HNO_3 plot (Plate 5), and is seen to affect the HNO_3 distribution up to at least ~600 K. In the "collar" region along the vortex edge, the HNO_3 contours dip sharply downward, as a result of strong descent. There is no obvious indication of denitrification in the AT-2 Arctic observations; this does not rule out the occurrence of a small amount of denitrification, but any effect of more than ~1 ppbv would be expected to be immediately apparent in Plate 5d. The downward tilt of the HNO_3 contours reflects the effects of descent in the vortex, and indicates the pattern of HNO_3 that would be expected in the spring vortex in absence of significant denitrification.

In the fall hemisphere, HNO_3 at the level of its maximum was greater during AT-3 than during AT-2, as expected for measurements taken later in the season [e.g., *Austin et al.*, 1986]. However, the AT-1 fall maximum HNO_3 values were substantially higher than those during AT-2 or AT-3. This is consistent with the enhancement in HNO_3 due to heterogeneous reactions on sulfate aerosols after the Mount Pinatubo eruption [*Koike et al.*, 1994; *Kumer et al.*, 1996].

Finally, in Plate 6 we show the EqL/θ space distribution of O_3 observed by ATMOS during the ATLAS missions. As expected, there is widespread O_3 depletion in the Antarctic lower stratospheric vortex during AT-3. In the absence of chemical depletion in the lower stratosphere, O_3 mixing ratios are substantially higher inside than outside the vortex below ~600 K [e.g., *Manney et al.*, 1995a, and references therein]; thus, the comparable values seen inside and outside the Arctic lower stratospheric vortex during AT-2 are indicative of chemical O_3 loss, consistent with previous studies of that winter [*Manney et al.*, 1995c; *Michelsen et al.*, 1998b, and references therein]. Since descent masks chemical O_3

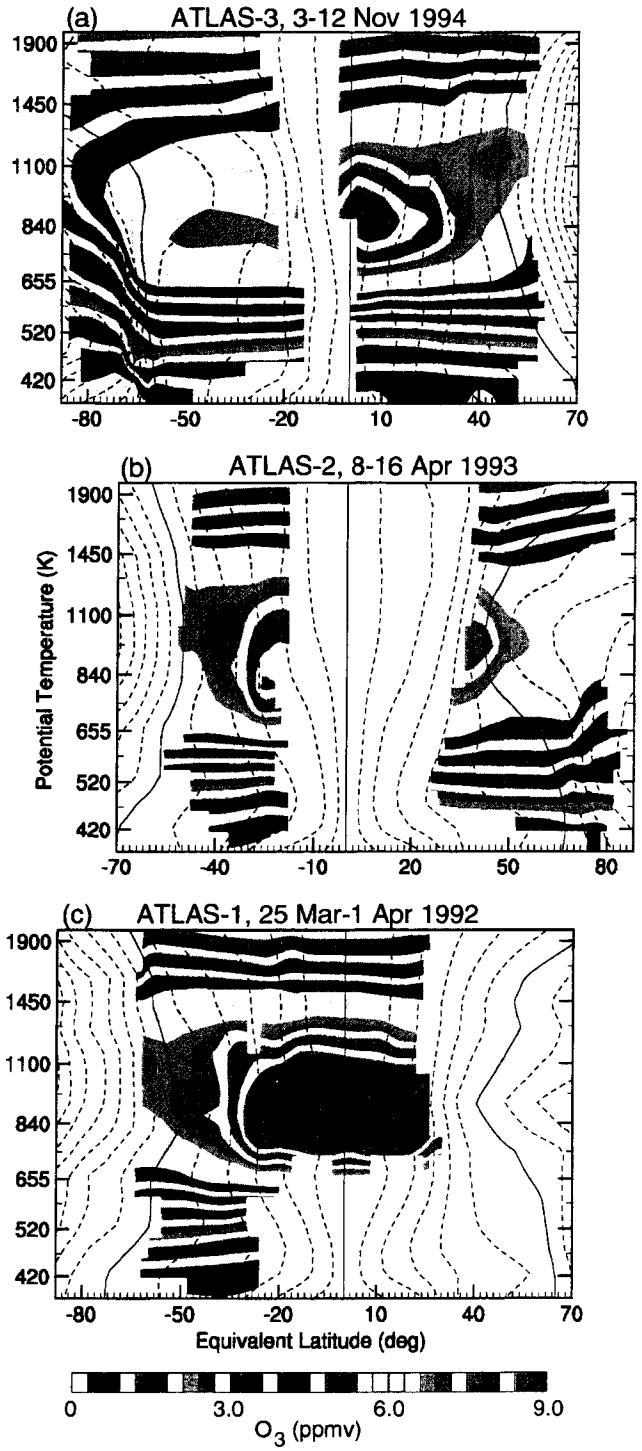

Plate 6. EqL/θ space fields of ATMOS O_3. Layout is as in Plate 3.

loss in the vortex, O_3 depletion occurred up to higher altitudes than is immediately apparent; previous studies of the 1992-93 winter indicate some O_3 depletion up to ~550 K [e.g., *Manney et al.*, 1995c, and references therein].

The main source of O_3 is in the tropical middle stratosphere, with mixing ratios exceeding 10 ppmv in the equatorial regions near 30–35 km [e.g., *Brasseur and Solomon*, 1986], high mixing ratios extending into midlatitudes in the middle stratosphere as air is transported poleward, and very strong gradients across the vortex edge as that air encounters a barrier to further poleward transport [e.g., *Manney et al.*, 1995a, and references therein]. The poleward and upward tilt of the level of peak mixing ratios seen in Plate 6 is characteristic of the early winter O_3 distribution, and has been attributed to a combination of photochemical and vertical transport processes [e.g., *Manney et al.*, 1995a, and references therein]; in monthly mean values shown by *Randel and Wu* [1995], this pattern is not well developed until November (May) in the NH (SH), suggesting that the stronger pattern during AT-3 is due to the later observation time.

Given the expected distribution and sources of O_3, the ATMOS values during AT-3 in SH middle EqLs look decidedly peculiar, and are in fact in disagreement with values observed by UARS MLS during this period. The reason for this discrepancy provides a note of caution in interpreting EqL/θ space plots of chemically active species. Examination of maps of MLS O_3 in the SH middle stratosphere during AT-3 (Plate 7) shows that many of the ATMOS observations at low EqL (i.e., low PV, solid contours) were taken in or near a "low ozone pocket" [*Manney et al.*, 1995b]; ATMOS O_3 profiles taken in the low ozone pocket region show the local minimum at the level of the O_3 maximum that is characteristic of this phenomenon. Such low ozone pockets form in the middle stratosphere near the level of the O_3 maximum when low-latitude, high-O_3 air is drawn poleward and confined for a number of days in the anticyclone, and O_3 mixing ratios in this confined air decrease rapidly in a manner that is inconsistent with the sole effect of transport processes [*Manney et al.*, 1995b]. *Morris et al.* [1998] and *Nair et al.* [1998] showed that the O_3 decrease is caused by a relaxation (via known chemical mechanisms) to an equilibrium value characteristic of high latitudes, since the air in the anticyclone is, in contrast to other midlatitude air, confined at relatively high latitudes for a sustained period. Low ozone pockets are common in the Arctic winter, and have been observed previously in the Antarctic late winter when wave activity was strong [*Manney et al.*, 1995b]. Plate 7 shows that most of the ATMOS observations that sampled higher O_3 values characteristic of midlatitudes and the subtropics were actually taken at higher PV than those in the low ozone pocket

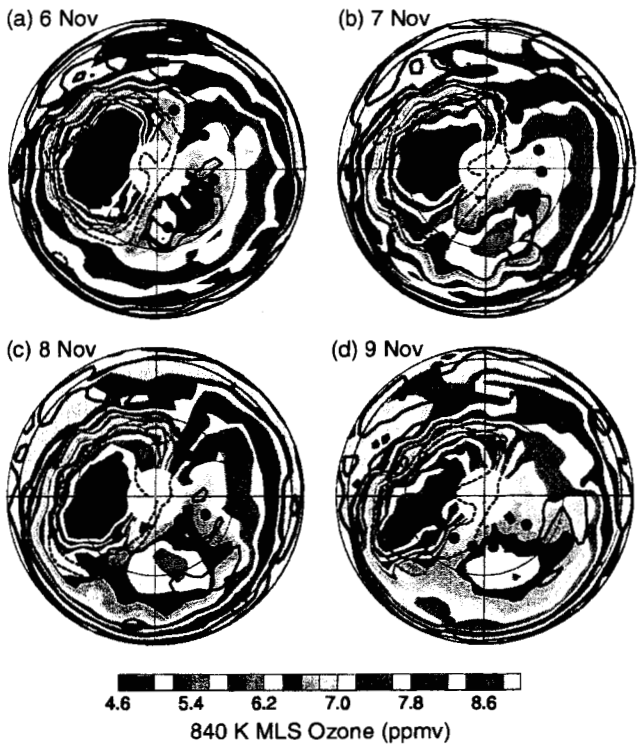

Plate 7. Maps of MLS O_3 in the SH on the 840 K isentropic surface during the AT-3 mission. |sPV| contours are overlaid in black; 1.2 and 1.4 $\times$ 10^{-4} s^{-1} contours are dashed, 0.6 and 0.8 $\times$ 10^{-4} s^{-1} contours are solid. The black dots show the locations of ATMOS observations on each day. The map projection is orthographic, with 0° longitude at the top and 90°E to the right. The domain is from equator to pole, with thin dashed lines at 30 and 60°S.

– these observations are in the entrance region where low-latitude air is drawn up around the vortex, and O_3 gradients are very strong. Thus Plate 6 shows lower rather than higher O_3 at lower EqLs, and even the highest values shown are an average including a substantial fraction of measurements from in or near the low ozone pocket.

4.2. Derived Fields and Indications of Mixing

A number of quantities derivable from the ATMOS observations are useful in clarifying aspects of dynamical and chemical processes in the stratosphere.

The quantity $\mathbf{H} = H_2O+2CH_4$ represents the variable part of total hydrogen, since H_2 is nearly constant in the lower and middle stratosphere [e.g., *Jones et al.*, 1986]. **H** is expected to be conserved in the lower and middle stratosphere outside the tropics and regions of polar dehydration [e.g., *Abbas et al.*, 1996, and references therein]. Indeed, Plate 8 shows **H** from ATMOS observations to be 7.0–7.4 ppmv nearly everywhere between ~550 and 1400 K during AT-2 and AT-3, and slightly lower during AT-1. In this region, neither descent nor mixing will change **H** due to the lack of gradients (and descent from levels above ~1400 K would serve only to increase **H**). Thus the marked reduction in **H** in the Antarctic lower stratosphere allows us to say with confidence that dehydration in the SH vortex extended up to ~600 K, as was also indicated by *Rinsland et al.* [1996a]. Above ~500 K the decrease in H_2O was masked in Plate 5 by descent of higher H_2O. The spreading of low **H** outside of the region of strongest PV gradients at the lowest levels shown also suggests greater permeability of the vortex below ~420 K, consistent with a number of theoretical calculations [e.g., *Manney et al.*, 1994c].

A decrease of ~0.6–0.8 ppmv in **H** was seen in the Arctic vortex during AT-2 (Plate 8b) below ~500 K, consistent with values calculated for vortex averages by *Michelsen et al.* [1999]. *Michelsen et al.* [1999] showed that this decrease was consistent with observations made several weeks later during the Stratospheric Photochemistry, Aerosols and Dynamics Expedition (SPADE) aircraft mission in vortex fragments. They suggested that this may be due to dehydration, or alternately, to descent of mesospheric air. Although the Arctic vortex was sufficiently eroded during AT-2 that one cannot judge from AT-2 data whether mesospheric air had been present in the stratospheric vortex [*Abrams et al.*, 1996c], given that lower mesospheric air descends only to ~600 K in the SH [*Schoeberl et al.*, 1995; *Abrams et al.*, 1996a, and references therein] where the period of unmixed descent is much longer, descent of mesospheric air to below 500 K in the Arctic seems at best a remote possibility.

Below 500 K in low and middle EqLs in the fall hemisphere, Plate 8 shows higher **H** in November during AT-3

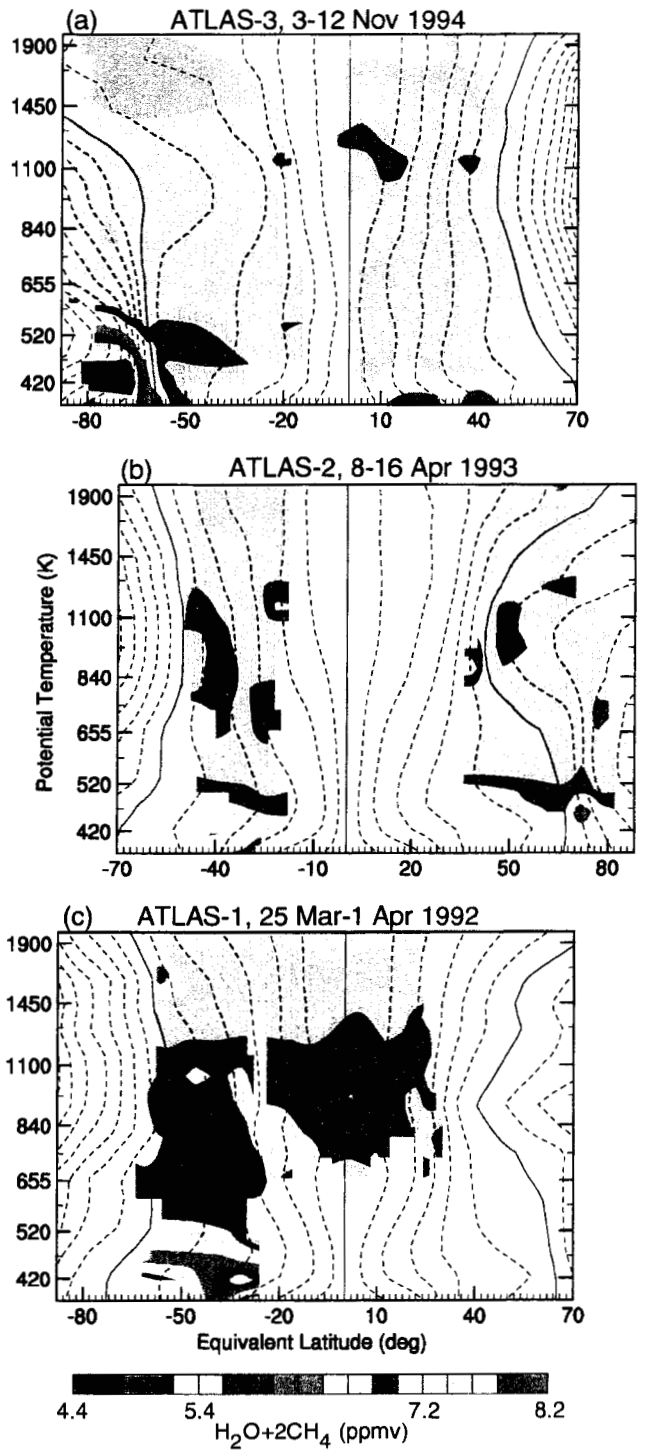

Plate 8. EqL/θ space fields of ATMOS H_2O+2CH_4. Layout is as in Plate 3.

than in March/April during AT-2 and AT-1. The difference in **H** results from differences in H_2O in these regions (Plate 5) and is probably related to the seasonal cycle in H_2O entering the stratosphere [e.g., *Mote et al.*, 1996, and references therein]. Allowing for a delay of several weeks between tropics and midlatitudes, the values shown here are consistent with the timing of the seasonal cycle in H_2O in the tropical lower stratosphere shown by *Mote et al.* [1996] in HALOE and SAGE II data. H_2O (Plate 5) and **H** (Plate 8) showed an overall increase throughout the stratosphere between AT-1 and AT-2 (~2.5 y), qualitatively consistent with recent trend studies [*Oltmans and Hofmann*, 1995; *Nedoluha et al.*, 1998a, b; *Evans et al.*, 1998; *Randel et al.*, 1999]. *Randel et al.* [1999] found ~1%/y increase throughout the stratosphere in **H** over a period including the ATLAS missions, consistent with the amount of increase seen in the ATMOS data.

Regions of enhanced mixing of vortex and extravortex air in the middle to lower stratosphere can be revealed by examining CH_4-CH_4^* (Plate 9). CH_4^* is analogous to the commonly-calculated NO_y^* [e.g., *Fahey et al.*, 1990a; *Sugita et al.*, 1998; *Kondo et al.*, 1999, and references therein], i.e., it is the expected CH_4 obtained from a polynomial relationship for midlatitudes between CH_4 and N_2O. We use the relationship given by *Michelsen et al.* [1998a]; they showed that because there is a nonlinear relationship between N_2O and CH_4 for $N_2O \lesssim 200$ ppbv for fall midlatitude and protovortex air, the mixing of air that had descended in the vortex with extravortex air produced a change in the CH_4/N_2O relationship for air defined as being within the vortex. Since there were not significant chemical changes in CH_4 in the lower stratospheric polar vortices, the primary source of changes in the CH_4/N_2O correlations was mixing of vortex (originally from high altitudes) and extravortex (from low altitudes) air. Thus, Plate 9 indicates regions where there was mixing of descended vortex air with extravortex air. In the SH during AT-3 (Plate 9a), the strongest signature of mixing was along the edge of the vortex at levels where it was strongly eroded, ~600–900 K. Below ~700 K, there was a small region in the vortex core that showed less evidence of mixing, consistent with previous studies, which showed mixing with extravortex air took place along the Antarctic vortex edge but not deep in the interior [e.g., *Bowman*, 1993; *Manney et al.*, 1994c]. Below 420 K, mixing would not affect the CH_4/N_2O relationship since N_2O values were sufficiently high both inside and outside the vortex that the two initial air masses would fall along a nearly linear part of the correlation curve.

In the Arctic during AT-2 (Plate 9b), the air in the vortex below ~800 K had experienced mixing, with the greatest changes seen in the vortex interior between about 500 and

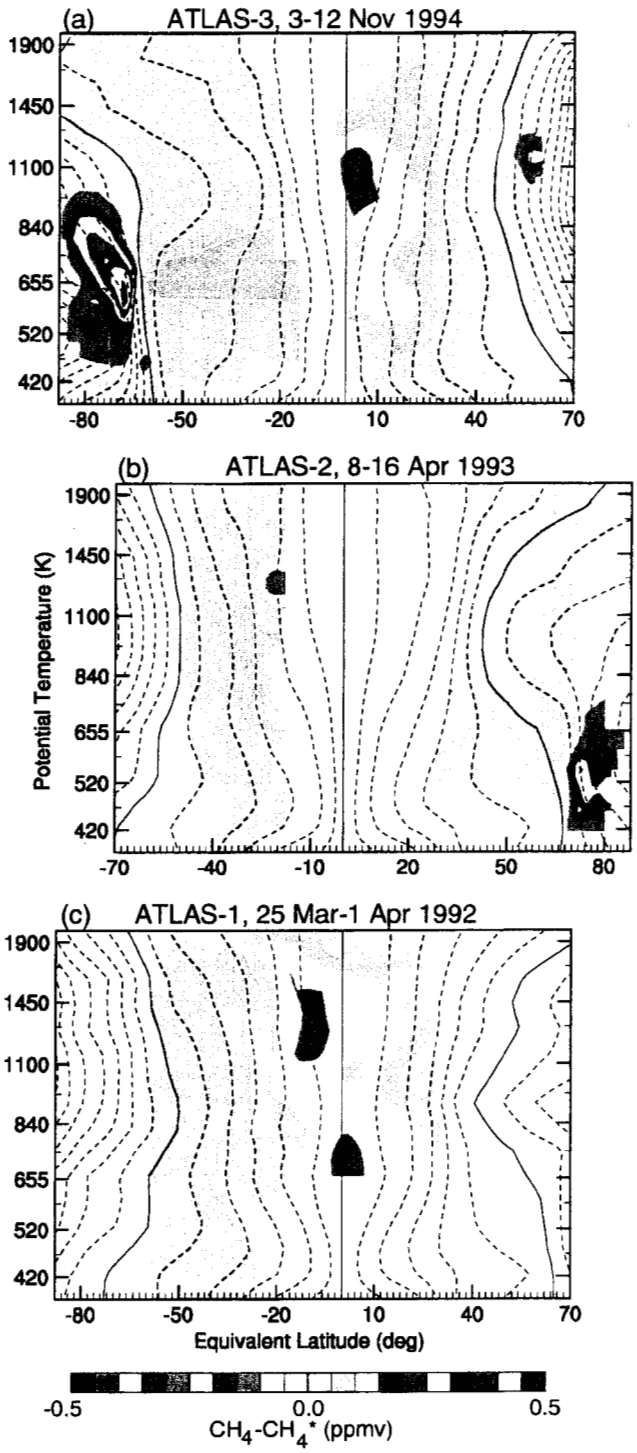

Plate 9. EqL/θ space fields of ATMOS CH_4-CH_4^* (see text). Layout is as in Plate 3.

600 K. A given deficit in CH_4-CH_4^* represents more mixing in the NH plot than in the SH plot; since the N_2O gradients were weaker in the NH, air masses that are separated by the same physical distance are represented by points more closely spaced around the nonlinear portion of the correlation curve and mixing between them thus produces a smaller change. Although we expect that mixing was occurring in middle to high EqLs between ~800 and 1100 K given the dynamical situation with large portions of the vortex being shredded off into midlatitudes, the uniformly low N_2O values at these levels (Plate 3c) suggest that mixing would not cause large deviations from the canonical CH_4/N_2O correlation and thus would not be evident on the CH_4-CH_4^* map.

Total reactive nitrogen, NO_y, calculated as $HNO_3 + NO + NO_2 + ClONO_2 + 2N_2O_5 + HNO_4$, and NO_y-NO_y^* are also useful for examining aspects of transport and chemistry in the polar stratosphere [e.g., *Michelsen et al.*, 1998b; *Rinsland et al.*, 1999, and references therein]. Plate 10 shows NO_y calculated from the ATMOS data. *Michelsen et al.* [1998b] provided polynomial fits to correlation curves between NO_y and N_2O for the tropics, the midlatitudes in fall, the high-latitude extravortex region in spring, the proto-vortex, and the Arctic vortex. We use the proto-vortex relationship to calculate NO_y^* and NO_y-NO_y^* (Plate 10). The proto-vortex relationship is used because it is the best estimate of a middle to high latitude relationship uninfluenced by tropical/subtropical or vortex air. Also, the proto-vortex correlation curves derived for AT-2 in the SH and AT-3 in the NH are nearly the same for $N_2O \gtrsim 40$ ppbv [*Michelsen et al.*, 1998b]. NO_y-NO_y^* obtained using the relationships for NO_y^* given by *Sugita et al.* [1998] and *Kondo et al.* [1999] (who used a relationship derived from AT-3 NH observations including proto-vortex, midlatitude, and low-latitude air) is qualitatively similar, with small quantitative differences in the middle EqL upper and lower stratosphere.

In the lower stratosphere, NO_y in the Antarctic spring vortex was depleted, reflecting the substantial denitrification that was evident in Plate 5. NO_y was enhanced relative to that outside the vortex along the edge of the Antarctic lower stratospheric vortex during AT-3, and inside the Arctic lower stratospheric vortex during AT-2, reflecting the effects of diabatic descent. This is consistent with the HNO_3 shown in Plate 5, as expected since HNO_3 is the primary component of NO_y at these levels. The net source of NO_y is oxidation by $O(^1D)$, which increases with increasing altitude; above about 30 km there is fast loss via the reaction $NO+N \rightarrow N_2+O$ [e.g., *Michelsen et al.*, 1998b]. These reactions, combined with ascent in the tropics, poleward and downward transport in the winter hemisphere, and mixing in midlatitudes, result in the overall pattern of NO_y with a maximum in the tropical middle stratosphere. The minimum in the Antarctic during AT-3 near 840 K and the maximum just below it may be a remaining signature of descent in the vortex. *Callis et al.* [1996] indicated that the enhanced NO_y-NO_y^* shown by *Rinsland et al.* [1996a] (corresponding to the region of higher NO_y in Plate 10a at highest EqLs between ~600 and 800 K) was consistent with their 2-D model results for conditions of enhanced NO_y production in the thermosphere (these comparisons are discussed further by *Rinsland et al.* [1999]).

As expected from comparing the overall distributions of NO_y (Plate 10) and N_2O (Plate 3), the fall correlation curves between N_2O and NO_y are nonlinear for low N_2O, with a maximum in the curve near $N_2O \approx 50$ ppbv [e.g., *Michelsen et al.*, 1998b]. Thus, where air masses from points on either side of the maximum are in close physical proximity (such as inside and outside the spring polar vortices), changes in the correlation curve, indicated in Plate 10 by departures of NO_y-NO_y^* from zero, can result from mixing between those air masses [*Waugh et al.*, 1997]. Departures of NO_y-NO_y^* from zero may also be caused by anomalous chemistry, and changes in N_2O/NO_y correlations have frequently been used to infer denitrification in the lower stratospheric vortices [e.g., *Michelsen et al.*, 1998b; *Kondo et al.*, 1999, and references therein]. *Michelsen et al.* [1998b] showed that most of the difference between the AT-2 Arctic vortex and midlatitude (or proto-vortex) NO_y/N_2O correlations could be explained by mixing across the vortex edge; they also showed that approximately half of the NO_y deficit apparent in the Antarctic vortex NO_y/N_2O correlation curve for AT-3 could be attributed to mixing. Vortex and extravortex air masses will fall on the canonical NO_y/N_2O correlation curve in positions that span a nonlinear section of the curve for vortex $N_2O \lesssim 50$ ppbv and extravortex $N_2O \gtrsim 50$ ppbv. Examination of individual N_2O profiles shows that these conditions were fulfilled between ~510 K and 900 K in the SH during AT-3 and between ~475 K and at least 900 K during AT-2. Thus we can expect the effects of mixing to be visible in NO_y-NO_y^* at least at these levels. Mixing may in fact affect these curves at somewhat higher and lower levels, since these estimates were based on fields that had already experienced some mixing; previous mixing would have increased the values in the lower stratospheric vortex and decreased those in the midlatitude middle stratosphere. The effects of earlier mixing are expected to be much larger in the NH than in the SH, since many studies [e.g., *Plumb et al.*, 1994; *Manney et al.*, 1994c, and references therein] have shown evidence of intrusion of extravortex air into the NH lower stratospheric vortex during the winter, and the Arctic vortex in the middle stratosphere was strongly disturbed in February and March 1993 [e.g., *Manney et al.*, 1994c], suggesting previous mixing there as well.

Plate 10 shows the morphology of the regions of de-

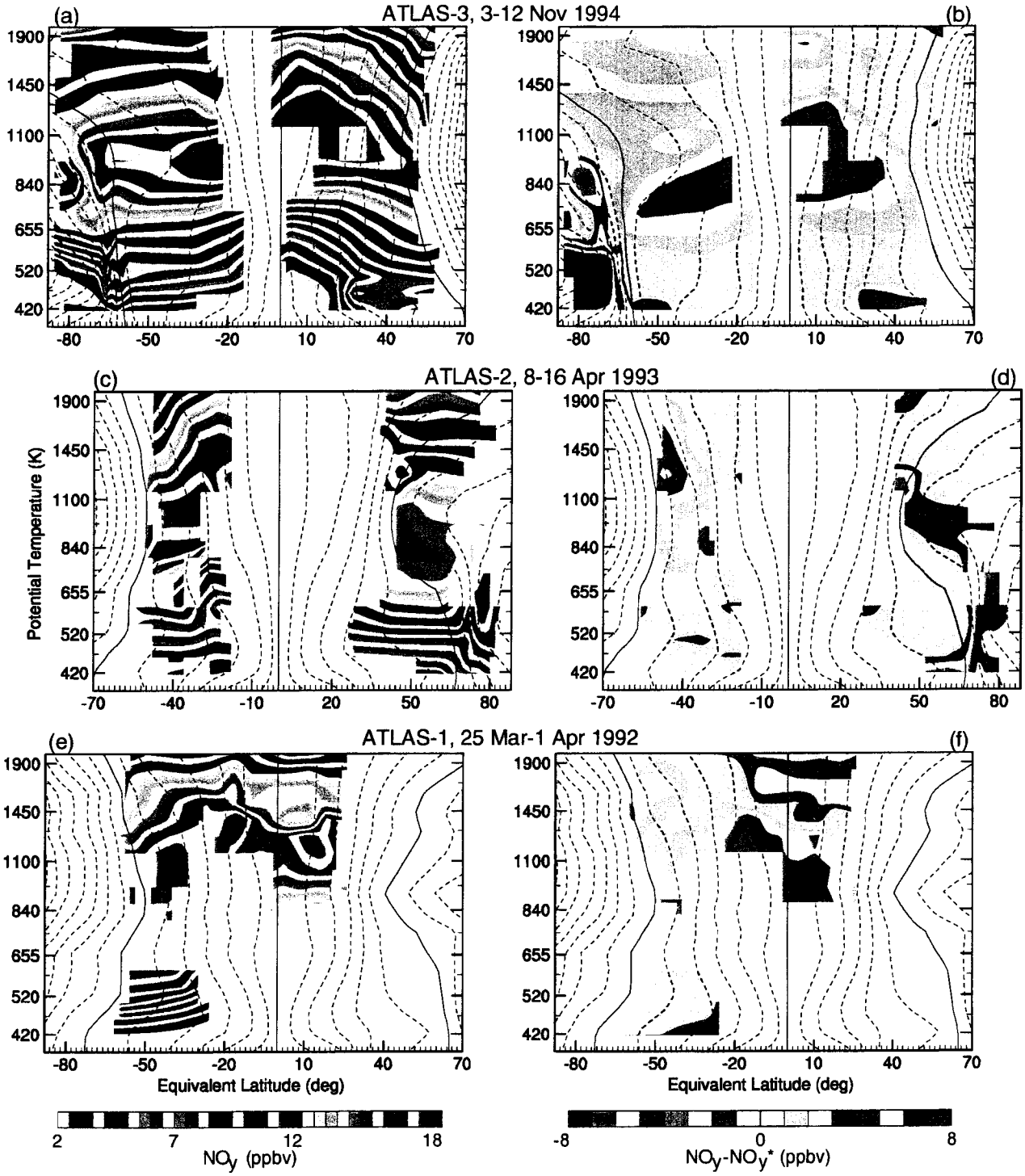

Plate 10. EqL/θ space fields of ATMOS NO_y (left) and NO_y-NO_y^* (right). Layout is as in Plate 3.

pressed NO_y-NO_y^* that result from the difference between springtime-vortex and proto-vortex correlations. The region of depleted NO_y-NO_y^* along the vortex edge during AT-3 is consistent with the effects of mixing. The region of enhanced NO_y-NO_y^* between ~600 and 800 K was confined to the vortex interior, where Plate 9 suggested little mixing with extravortex air. Below about 500 K, N_2O values were sufficiently high inside the vortex that mixing would produce little change in the NO_y/N_2O relationship. Thus, most of the depression in NO_y-NO_y^* in the Antarctic vortex below 500 K can be attributed to denitrification. Although we have shown that some mixing occurred above 500 K, denitrification is also expected at these higher levels. Plate 8 showed that dehydration extended up to at least about 600 K. Since HNO_3 is expected to fall out as well as H_2O when water ice PSCs sediment, it is expected that denitrification extended at least as high as dehydration, consistent with the vertical extent of the region of most strongly depressed NO_y-NO_y^* in Plate 10. Since at this level (near 600 K) the effects of mixing, and likely effects of earlier descent of mesospheric air, are present, we are unable to determine from these data whether denitrification in fact extended any higher than dehydration.

In the Arctic vortex during AT-2, N_2O values were low enough and gradients across the vortex edge strong enough that NO_y-NO_y^* would be altered due to mixing at levels down to at least 475 K; mixing would probably be apparent at somewhat lower levels, since considerable mixing that occurred prior to AT-2 [e.g., *Manney et al.*, 1994c] had already increased the N_2O mixing ratios in the vortex. It is difficult to define a top level where extravortex N_2O was greater than 50 ppbv during or prior to AT-2, due to the large area of coverage of air either currently or recently inside the vortex in the middle stratosphere (Section 2). Comparing the Arctic lower stratospheric vortex region with the region of mixing indicated in Plate 9, and given that it is not necessary to invoke denitrification to explain the vortex NO_y/N_2O correlation during AT-2 [*Michelsen et al.*, 1998b], the decrease in NO_y-NO_y^* below ~800 K leads us to believe that mixing with extravortex air took place throughout the portion of the vortex observed by ATMOS. A signature of mixing can also be seen from 800–1100 K; this was not evident in Plate 9 because the canonical NO_y/NO_y^* correlation is much more sharply peaked than that for CH_4 and N_2O; the effects of mixing are apparent in this region where the gradients in N_2O between vortex and extravortex observations were relatively weak, and thus mixing did not change the CH_4/N_2O correlation significantly.

4.3. Parcel History Calculations

The above results showed how the ATMOS data reflect transport processes associated with the evolution of the polar vortex. Here we present the results of trajectory calculations (Section 3.3) to examine the consistency of the calculated recent history with the morphology of the ATMOS tracer fields.

Plate 11 summarizes the vertical motion experienced by the air measured by ATMOS in the 32 days prior to each ATLAS mission. Consistent with the calculations of *Manney et al.* [1994c], strong descent was still occurring in the spring middle stratosphere, although there was net ascent in the upper stratosphere. Stronger ascent in the spring upper stratosphere during AT-3 than during AT-2 was likely due to the AT-3 observations being later in the season. The values shown here represent the calculated descent of the air sampled by ATMOS averaged in PV/θ bins. The region of stronger but more localized descent in the SH middle stratosphere during AT-3 than in the NH middle stratosphere during AT-2 reflects greater confinement of air in the SH vortex; although cooling rates are not larger overall in the SH, greater confinement means that air that experienced strong descent in the vortex has not been mixed with less-descended midlatitude or subtropical air. The abrupt increase in descent in crossing from extravortex to vortex at levels below 840 K (where the vortex is still well-defined) in both hemispheres also indicates a greater uniformity of the averaged air within the vortex, since the cooling rates themselves do not increase dramatically across this boundary. That this increase is stronger in the SH than in the NH reflects the greater degree of impermeability of the Antarctic vortex.

The effects of confinement in the vortex, or in vortex remnants, are apparent in the standard deviation of $\Delta\theta/\Delta t$. While, all other things being equal, larger standard deviations would be associated with larger descent rates, the differences in the locations of maximum descent and largest variance are informative. In the SH middle stratosphere the location of largest variance is above and toward the vortex edge of the maximum descent, indicating more mixing of air with differing descent rates along the vortex edge and where the vortex is more eroded. A similar pattern occurs in the NH. An increase in the standard deviation along the vortex edge in the SH extends only down to about 650 K, below which the vortex is still quite strong, suggesting greater mixing along the vortex edge at levels where it has been eroded. Both Arctic and Antarctic vortices show more descent along the vortex edge in the lower stratosphere, consistent with previous studies [*Schoeberl et al.*, 1992; *Manney et al.*, 1994c]. The descent rates at the lowest levels shown are near zero in the NH vortex, but in the SH there is ascent of $\lesssim$0.4 K/d in the interior of the Antarctic vortex (in the

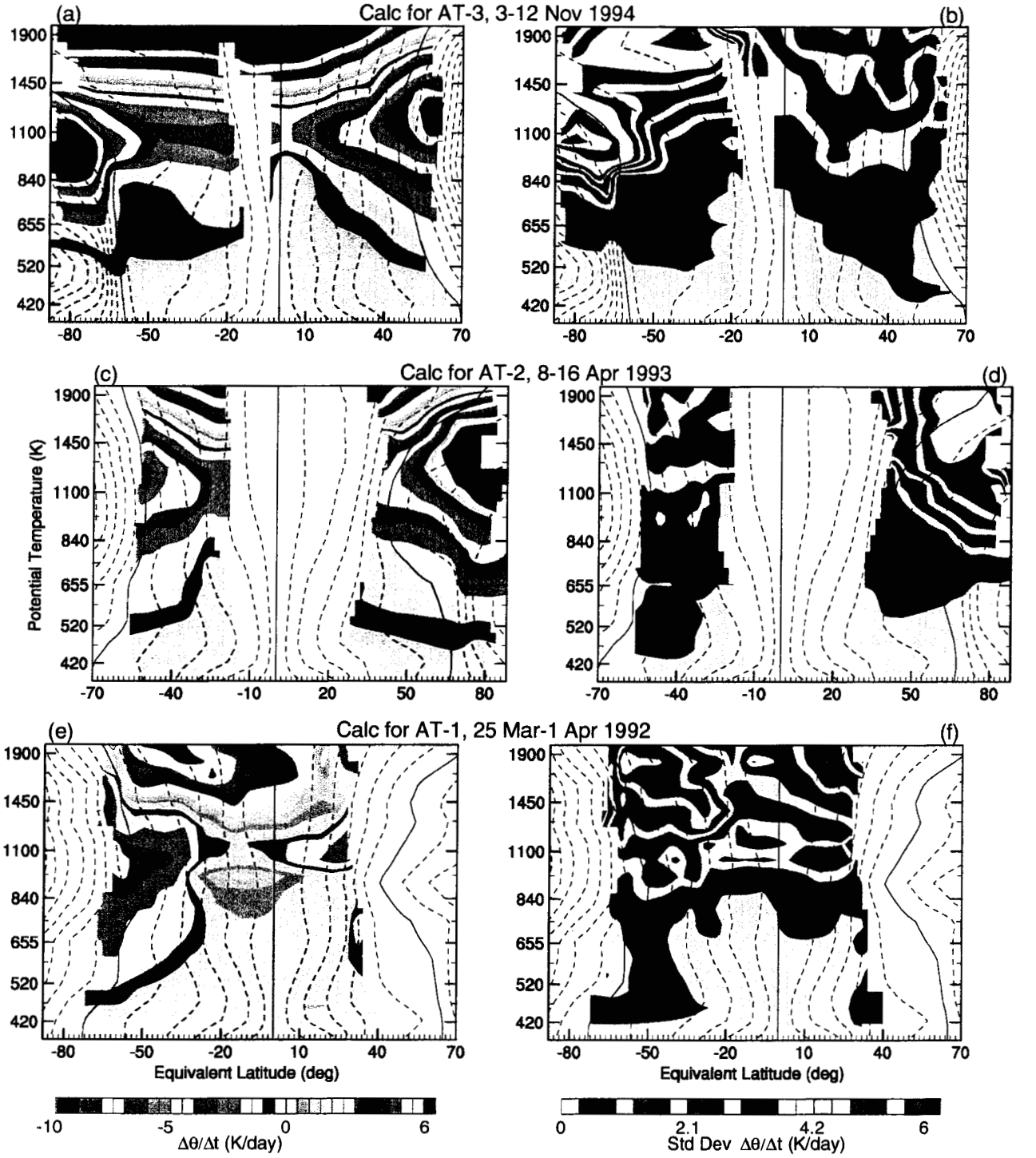

Plate 11. EqL/θ space fields of the change in potential temperature (left) and the standard deviation of that change (right) calculated for parcels initialized in columns at the latitude and longitude of each ATMOS observation (see Section 3.3), from 32-day back-trajectory calculations. The change in potential temperature is expressed in K/d by dividing the change for each parcel by 32 before gridding in EqL/θ space. Layout is as in Plate 3.

grey contour region in Plate 11). Enhanced descent along the edge of the lower stratospheric vortex is consistent with the appearance of the ATMOS tracer fields (e.g., Plates 3 and 5).

In the fall hemisphere, a widespread region of descent is centered at highest EqL for each ATLAS mission, with stronger descent in each succeeding mission, as expected from the more advanced season of the later missions. That the variance decreases in the upper stratosphere at the highest EqL for AT-3 but not for AT-2 or AT-1 suggests that more of an effect of confinement in the proto-vortex is seen for the later time of the AT-3 mission.

Similar calculations were done examining the net horizontal motions of the parcels in the month before the ATLAS missions, by examining average changes and standard deviations in latitude, sPV, and EqL. The results of these calculations (not shown) have several features that are consistent with the overall picture of transport reflected in the ATMOS tracers: very large standard deviations along the vortex edge between ~600 and 900 K in the SH, and at all levels below ~900 K in the NH during AT-2; an increase in standard deviation in the NH during AT-2 at all EqLs between ~850 and 1100 K; a distinct decrease in standard deviations at the highest northern EqLs observed during AT-3, which is not readily apparent in the AT-2 or AT-1 fall observations.

To examine further the history of the air that ATMOS sampled, we calculated similar averages for the parcels from the 32-day histories, but plotted the historical values of trace gases (N_2O, CH_4, and H_2O) from the EqL/θ "climatologies" described in Section 3.4. Plate 12 shows the EqL/θ initialization fields for N_2O (Section 3.4) averaged over 8 days centered 32 days prior to the ATLAS missions, and the N_2O at the time of the ATLAS missions calculated from these initialization fields. Given the idealized nature of the initialization fields and possible biases between the ATMOS and UARS data [e.g., *Roche et al.*, 1996], we do not expect quantitative agreement between the calculated fields shown here and the ATMOS observations. The overall systematic differences between the calculated fields in Plate 12 (right-hand side) and the ATMOS N_2O shown in Plate 3 are, in fact, greatest during AT-3. This is not unexpected, since the fields used to initialize that case were derived from CLAES data from October 1992, whereas the CLAES data used to derive the initialization for AT-2 were from March 1993, the same year as AT-2 (Section 3.4. Interannual variability, which is large in both NH and SH spring, thus also contributes to making these initialization fields suitable mainly for qualitative comparisons. However, the changes between the initial and final fields are still instructive of the mechanisms that shaped the air masses sampled by ATMOS in the month immediately prior to those observations. Results for initialization with fields derived from CLAES CH_4 and MLS H_2O (not shown) are similar to those for N_2O.

Continuing descent along the vortex edge (Plate 11) leads to a decrease in N_2O values in the lower stratosphere; weak ascent in the vortex interior leads to a slight increase in the interior of the vortex (compare Plates 12a and b (SH) and Plates 12c and d (NH)). The pattern thus produced is consistent with the pattern seen more strongly in the ATMOS data (Plate 3). The history for the entire winter probably also contributes to the pattern seen in the ATMOS data, since in the lower stratosphere strongest descent is along the vortex edge throughout the winter in the SH and during the late winter (from February) in the NH [e.g., *Manney et al.*, 1994c]. In the SH upper stratosphere during AT-3, the poleward spread of higher N_2O values results from mixing as the polar vortex decays (the extent of the decay during this period can be seen by comparing the overlaid |sPV| contours between Plate 12a and Plate 12b). In the NH middle stratosphere during AT-2, spreading and poleward excursion of the N_2O contours indicate the strong mixing taking place there in the month preceding the AT-2 observations. This evolution of the vortices and associated tracer transport results in further steepening of the tracer gradients along the vortex edge in the lower stratosphere.

In the fall hemisphere during all three missions, increasing descent and confinement in the polar regions lead to downward motion of the tracer contours. This motion is most pronounced during AT-3, consistent with stronger descent and greater confinement during that mission. Note that during AT-2, a sharp bend in the N_2O contours develops between 520 and 655 K near 40°S EqL, reminiscent of a similar bend seen in the AT-2 data (Plate 3).

The standard deviation of the N_2O values comprising the average in each PV/θ grid box (Plate 13) gives information on the homogeneity of the history of air sampled by ATMOS. Enhanced mixing is apparent along the Antarctic vortex edge during AT-3 above about 600 K, along the Arctic vortex edge during AT-2 below ~840 K, and in most of the NH region between 840 and 1100 K during AT-2. Because the initial N_2O fields had weak horizontal gradients in the Arctic vortex during AT-2, the decrease in variance in the vortex interior does not necessarily indicate the absence of mixing, but does suggest that mixing during this period may have been limited to air from near the vortex edge, rather than having extravortex air transported deep into the vortex. Although the changes in ATMOS CH_4-CH_4^* (Plate 9) and NO_y-NO_y^* (Plate 10) reflect processes that occurred throughout the winter, there is fair agreement between the areas of enhanced mixing seen in ATMOS tracer relationships and the diagnostics of recent mixing shown here from the transport calculations.

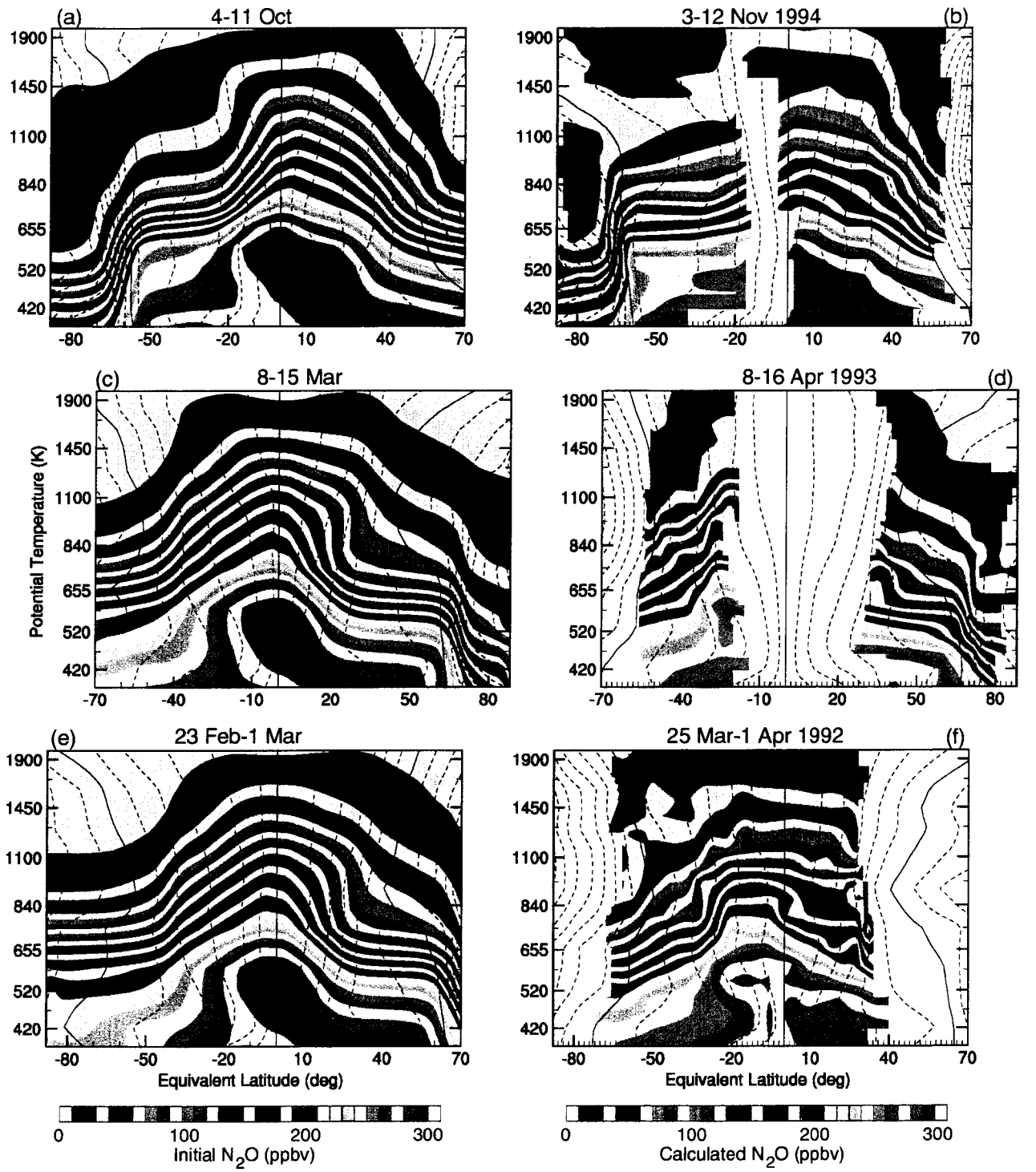

Plate 12. EqL/θ space fields of initialization N_2O data derived from CLAES observations (Section 3.4) (left) and N_2O calculated from these initialization fields for the time of the ATMOS observations (right). The transport calculations use parcels initialized in columns at the latitude and longitude of each ATMOS observation, as described in Section 3.3, and are 32 days long. Layout is as in Plate 3.

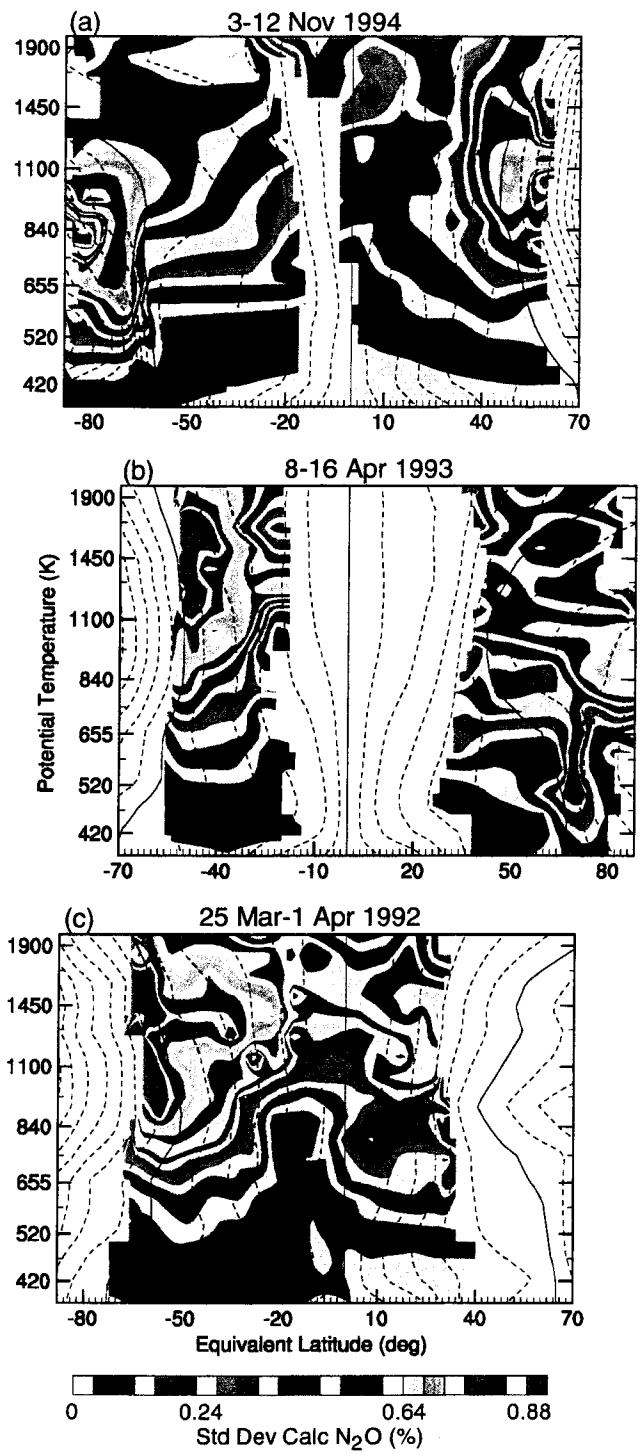

Plate 13. EqL/θ space fields of the standard deviation of the calculated N_2O shown in Plate 12; the standard deviation is normalized by the average (Plate 12, right side) to emphasize relative changes. Layout is as in Plate 3.

In the fall hemisphere, a region of increased variance in the high EqL upper stratosphere during each mission reflects the mixing of air that was drawn in around the proto-vortex and drawn off the proto-vortex edge. This region was more limited during AT-3 than during the previous missions, indicating a stronger transport barrier and more limited mixing during AT-3. Enhanced variance extending further out to low EqL during AT-1 than during AT-2 is consistent with the weaker and more distorted proto-vortex during AT-1 (Section 2).

We now look in more detail at the recent history of the air observed by ATMOS in the spring vortices and the fall proto-vortices. We show the positions (in PV and Δθ) and N_2O values (from the idealized UARS-based fields) of individual parcels that were in specified PV/θ bins at the time of the ATMOS observations. We also show the averages for groups of parcels initialized at the same level; the close correspondence between these averages (of 121 parcels each) and the individual parcels indicates that these displays are representative of the behavior of the ensemble of parcels.

Plate 14 shows such a plot at several levels for the AT-3 sunrise observation locations between -1.6 and -2.0 × 10^{-4} s^{-1} sPV; this range is inside the vortex, but still generally in the region of strong PV gradients, as can be seen in the sPV overlays on the EqL/θ plots. Below 445 K (Plate 14a), there was overall ascent, as mentioned above, with increasing descent with increasing altitude above that (Plates 14b, c and d). At levels below 485 K, the sPV that the parcels came from is limited to a small range closely centered on the values at the time of AT-3 (denoted by vertical bars), as in Plate 14a, indicating very limited mixing in this sPV range. Between ~500 and 800 K (including the ranges shown in Plates 14b and c), there is increasingly more mixing, with air having come from both well outside and well inside the vortex (both much lower and much higher |sPV|). Although the situation is somewhat similar at 800-875 K (Plate 14e), the majority of the air came from higher |sPV| values; at these levels, the major changes during the period were due to the strong erosion of the vortex, as can be seen in Plate 12.

Plate 15 shows similar plots in the lower stratosphere for locations deep inside the vortex ($|sPV| > 2.0 \times 10^{-4}$ s^{-1}) and along the vortex edge ($1.0 < |sPV| < 1.6 \times 10^{-4}$ s^{-1}). In the vortex interior (Plate 15a), ascent extends up to ~500 K, and limited mixing is indicated by the tight clustering of the parcels near the |sPV| region where AT-3 observed them. The slight extension of these parcels' positions toward lower |sPV| suggests some mixing with air from outside the vortex core, but there is no evidence of air from outside the vortex ($|sPV| < 1.0 \times 10^{-4}$ s^{-1}). Higher up in the vortex interior (Plate 15b), most parcels came from much higher |sPV|, reflecting substantial erosion of the vortex at these

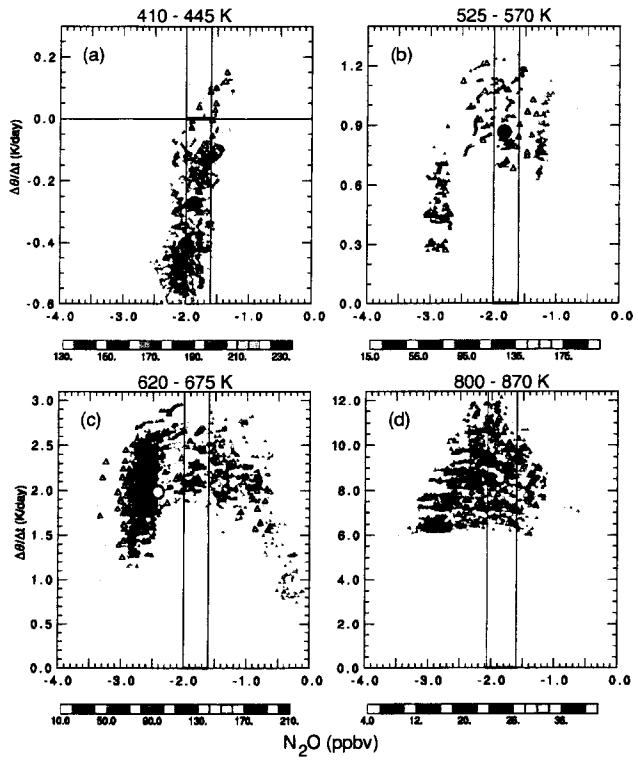

Plate 14. History of parcels for AT-3 sunrise (SH) observations with |sPV| between 1.6 and 2.0 $\times$ 10^{-4} s^{-1}. The x-axis is sPV (10^{-4} s^{-1}); the y-axis is the change in theta expressed in K/d by dividing the change for each parcel by 32 days, with positive values indicating descent (i.e., parcels that came from above their location at the time of the ATMOS observations appear above zero on the plot). Parcels are color coded by their N_2O mixing ratio (ppbv), calculated from the idealized UARS-based fields described in Section 3.4. Small colored triangles show individual parcels' positions 32 days prior to the ATMOS observations. Small black-bordered triangles represent the average for the 121 parcels initialized at a single level for each ATMOS profile (see Section 3.3). Large black-bordered circles represent the average position of all the parcels included. Vertical bars show the |sPV| range of the ATMOS profile locations that were included in each plot; the horizontal line shows zero theta change. Each theta range is chosen to include 5 of the 100 levels at which parcels were initialized, a vertical distance comparable to the ATMOS vertical resolution. Note that different N_2O color scales are used for each level, to emphasize the range of variations in N_2O .

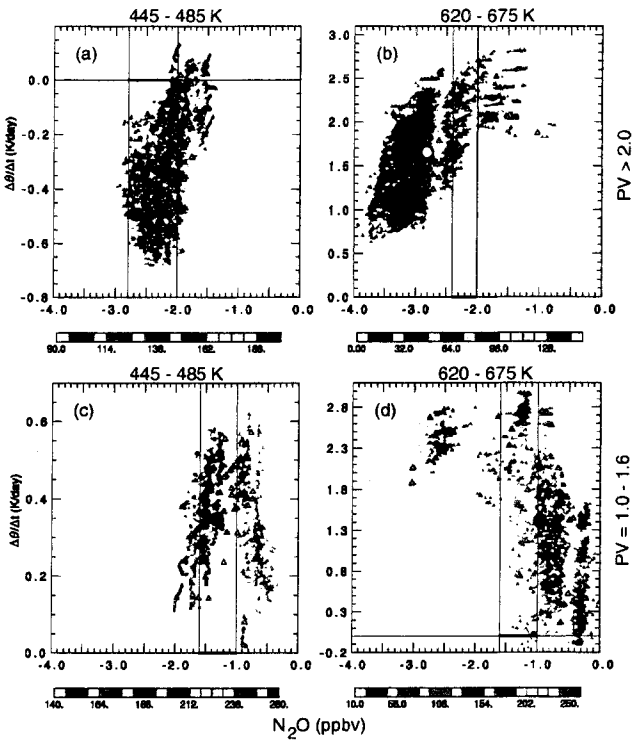

Plate 15. History of parcels at two levels for AT-3 sunrise (SH) observations with |sPV| greater than 2.0 $\times$ 10^{-4} s^{-1} (a and b, vortex core) and between 1.0 and 1.6 $\times$ 10^{-4} s^{-1} (c and d, vortex edge region). Layout is as in Plate 14.

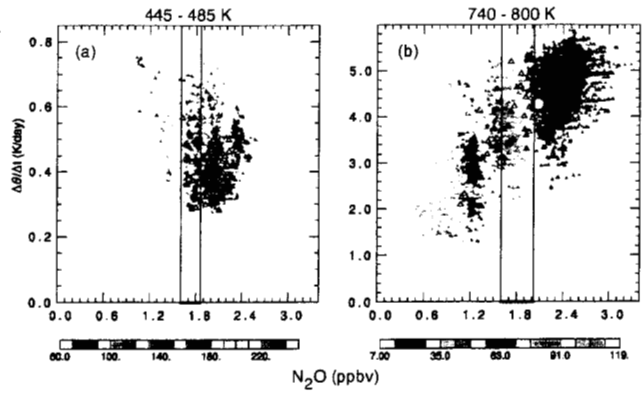

Plate 16. History of parcels at two levels for AT-2 sunrise (NH) observations with sPV greater than 1.6×10^{-4} s^{-1}. Layout is as in Plate 14.

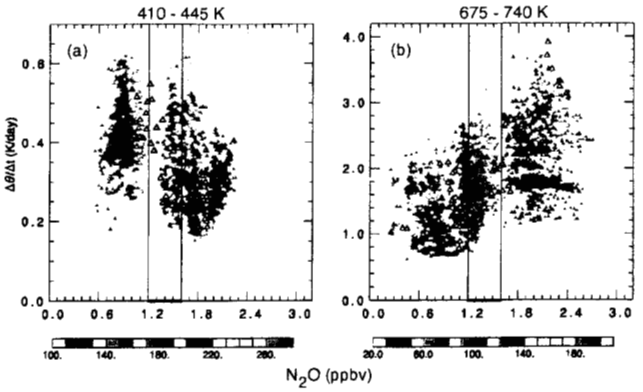

Plate 17. History of parcels at two levels for AT-2 sunrise (NH) observations with sPV between 1.2 and 1.6 $\times 10^{-4}$ s^{-1}. Layout is as in Plate 14.

levels in the month preceding AT-3. Along the vortex edge, a considerable amount of extravortex air mixes into the region down to at least 380 K (the lowest level studied) (Plate 15c shows 445-485 K), and there is continuing weak descent at these levels. Below ~420 K, the $1.0 < |sPV| < 1.6 \times 10^{-4}$ s^{-1}range extends further into the vortex interior, since the strongest PV gradients at those levels are at slightly lower |sPV| values; the presence of extravortex air in this |sPV| range at the lowest levels studied thus indicates mixing well into the vortex interior. At higher levels (Plate 15d), the air in the vortex edge region came from a wide range of sPV, both deep inside and well outside the vortex, with most of the air coming from lower |sPV| (outside the vortex); the air coming from the vortex interior experienced strong descent.

Plate 16 shows the origins of parcels that were at the locations of AT-2 observations in the interior of the Arctic vortex ($sPV > 1.6 \times 10^{-4}$ s^{-1}) in the lower and middle stratosphere. In contrast to the SH, there was still weak descent in the vortex interior during AT-2 below 500 K. There are indications of more mixing at these levels in the NH than in the SH during AT-3, with much of the air at the lowest levels shown here coming from deeper in the vortex, but some also coming from well outside the vortex (Plate 16a). At higher levels (Plate 16b), there is strong mixing in this region, with large portions of the air coming from both deep in the vortex and from the vortex exterior.

Plate 17 shows similar plots for air along the vortex edge and in the outer part of the vortex ($1.2 < sPV < 1.6$). The spread in the parcel positions indicates strong mixing at all levels where the vortex can still be defined. There was considerably more mixing of both extravortex and inner-vortex air at the lowest levels (below 500 K) in the NH during AT-2 than in the SH during AT-3.

Finally, we compare the parcel history in the fall proto-vortex edge region ($1.0 < |sPV| < 1.2 \times 10^{-4}$ s^{-1}) for the three ATLAS missions (Plate 18). At all the levels shown, most of the parcels (during all three missions) came from lower |sPV| since PV values within the developing vortex are increasing. Since AT-2 had less coverage of the proto-vortex than did AT-1 and AT-3 (e.g., Section 2), some differences between AT-2 and the other missions are expected; however, these differences, while resulting from sampling rather than physical effects, should be reflected in the ATMOS observations. In the middle to lower stratosphere (Plates 18a, b and c show 675–740 K), the histories were similar for all three missions, with nearly equal average descent, strongest descent in parcels from higher |sPV|, and similar ranges of N_2O. Between 870 and 950 K (Plates 18d, e and f), a difference in the descent rates between the three missions is apparent, with slightly greater average descent during AT-3 than during AT-2, and greater descent during AT-2 than during AT-1. The difference in descent between AT-3 and AT-1 was even more pronounced in the upper stratosphere (e.g., Plate 18g, h and i), although there is still only a slight difference between AT-3 and AT-2. Above ~870 K during AT-1 (Plates 18f and i), there were parcels in the proto-vortex edge region that had come from the tropics (near zero sPV) and that had experienced net ascent along their paths in the month preceding AT-1. Although AT-3 also observed parcels that originated in the tropics (Plates 18d and g), they had all experienced net descent over the previous month. AT-2 did not sample any tropical air in the proto-vortex region. This is related to the more symmetric and quiescent proto-vortex during AT-2 than during AT-3 and AT-1 (Section 2), which not only contributed to poorer sampling of

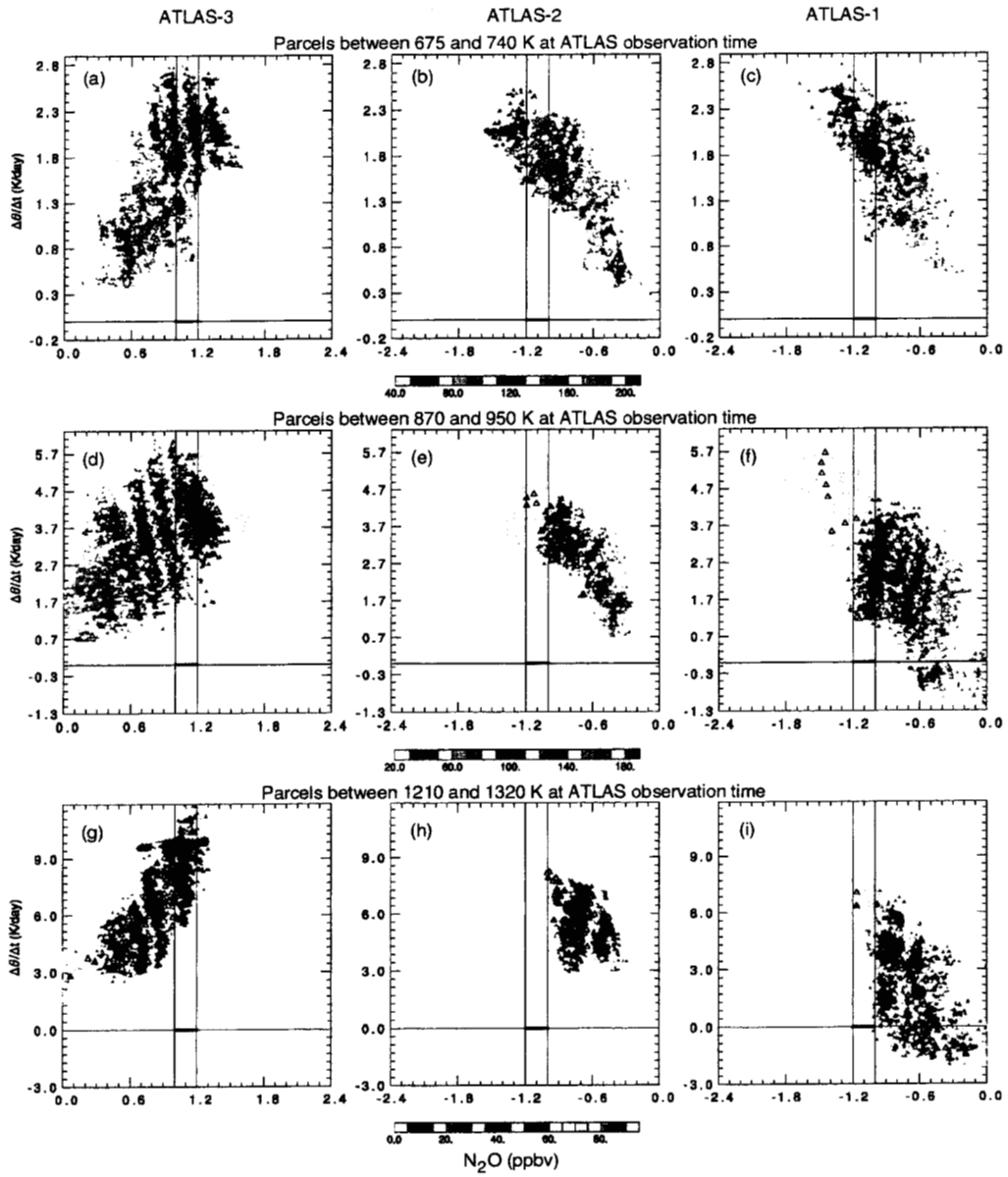

Plate 18. History of parcels with |sPV| between 1.0 and 1.2 × 10^{-4} s^{-1} for fall (sunset) observations during each of the ATLAS missions. Layout is as in Plate 14.

the proto-vortex, but also meant that less air was drawn into high latitudes from the tropics. Lowest average upper stratospheric N_2O values during AT-2 (Plate 18h) and highest during AT-1 (Plate 18i) are consistent with the relative N_2O values observed by ATMOS in the high-EqL upper stratosphere (Plate 3).

5. Summary and Conclusions

Trace gas fields measured by ATMOS during the three ATLAS missions have been mapped into equivalent latitude/θ space to examine how the tracer morphology is related to the evolution of the polar vortex. The highly distorted spring vortices result in coverage of subtropical to polar equivalent latitudes (EqLs). Although the fall proto-vortices are less asymmetric, there is enough distortion and variability to extend the coverage ~10° poleward in EqL from the highest geographical latitude observed. These fields, and similar mappings of derived fields (e.g., NO_y, H_2O+2CH_4, etc.), allow us to examine the effects of transport, mixing, and chemical processes in and around the polar vortex in more detail than previous studies. The ATMOS EqL/θ fields are compared with the results of back-trajectory calculations simulating the history of the air measured by ATMOS.

The EqL/θ fields of long-lived tracers in the spring hemisphere during AT-3 (3–12 Nov 1994) and AT-2 (8–16 Apr 1993) show the effects of descent that has taken place throughout the winter in the confined region of the polar vortex, as noted in previous studies [*Abrams et al.*, 1996a, c]. The net effect of strong descent in the upper stratosphere and decreasing descent with decreasing altitude is apparent in the packing of the tracer contours in the lower stratosphere. In addition, the EqL/θ mapped fields reveal evidence of greater descent at the edge of the lower stratospheric vortex than in the vortex center in both hemispheres, with tracer contours showing a downward excursion along the vortex edge. The results of trajectory calculations for the month prior to AT-3 and AT-2 are consistent with these patterns, showing continuing descent in the middle and upper stratosphere, and along the vortex edge in the lower stratosphere, with weak ascent in the SH lower stratosphere vortex interior during AT-3.

In the SH middle and upper stratosphere during AT-3, the region of low (descended) tracer values is confined more to a smaller region near the pole as altitude increases, indicating the effects of mixing and decay of the vortex. In the NH middle stratosphere during AT-2 the vortex was in the process of breaking down in a dramatic and untidy fashion, with a substantial portion of the vortex material pulled out into midlatitudes and mixed around and in the anticyclone. This process resulted in a spreading of low tracer values over a broad EqL range and weakening of vertical tracer gradients in the middle stratosphere.

Evidence of mixing in the spring lower stratospheric vortices is shown in variations of CH_4-CH_4^* and NO_y-NO_y^*, where CH_4^* and NO_y^* are calculated from fall midlatitude or proto-vortex correlations with N_2O [*Michelsen et al.*, 1998a]. The results show strong mixing in the SH during AT-3 above about 500 K, with the strongest mixing being confined to the vortex edge region between 500 and 700 K. Strong mixing is indicated throughout the AT-2 Arctic vortex below about 850 K. NO_y-NO_y^* indicates strong mixing between ~850 and 1100 K during AT-2 at all EqLs covered. Parcel history calculations for the month prior to the ATLAS missions show similar patterns of mixing. The trajectory calculations also indicate more widespread mixing in the SH middle stratosphere above ~900 K during AT-3. Detailed examination of parcel histories shows that air inside the vortex above about 500 K originated both deeper inside the vortex and well outside the vortex. Below that level, the calculations indicated little mixing of vortex interior with extravortex air during AT-3, although air near the vortex edge (inside) did mix with extravortex air down to 380 K. In the Arctic during AT-2, the trajectory calculations confirmed enhanced mixing along the vortex edge up to ~840 K, and at all EqL sampled by ATMOS above that. Detailed parcel histories showed extravortex air mixing well into the vortex above ~450 K, and into the vortex edge region down to 380 K.

Strong denitrification in the SH vortex during AT-3 is evident in the EqL/θ HNO_3 field, which suggested that denitrification extended up to at least ~600 K. The morphology of HNO_3 in the Arctic lower stratospheric vortex during AT-2 is consistent with the effects of descent. If denitrification greater than ~1 ppbv had occurred, its effects should be visible in this plot; thus the EqL/θ mapped HNO_3 field during AT-2 suggests that there was not significant denitrification during the 1992-93 Arctic winter, consistent with previous studies [e.g., *Michelsen et al.*, 1998b; *Santee et al.*, 1999, and references therein]. Since the NO_y/N_2O correlation is strongly affected by mixing over an even larger region than the CH_4/N_2O correlation, little additional information regarding denitrification is obtained by examining NO_y-NO_y^*. Large decreases in NO_y-NO_y^* in the interior of the Antarctic vortex below about ~600 K during AT-3 are likely due mainly to denitrification, although the decreases along the vortex edge at these levels may also result from mixing; below ~500 K the decrease can be attributed to denitrification, since none of the other diagnostics indicates substantial mixing into the vortex interior at those levels. During AT-2, in contrast, since there was other evidence of mixing throughout the Arctic lower stratospheric vortex, the decrease in NO_y -NO_y^* offers no unequivocal evidence of denitrification.

EqL/θ mapped H_2O fields show strong dehydration in the

Antarctic vortex during AT-3. Examination of H_2O+2CH_4 (which is unchanged by mixing and descent throughout the extratropical middle and lower stratosphere) indicates that Antarctic dehydration extended up to ~600 K during AT-3 and suggests the possibility of a small amount of dehydration in the Arctic vortex during AT-2 below ~500 K.

EqL/θ O_3 fields show strong O_3 depletion in the Antarctic spring vortex during AT-3 and evidence of O_3 loss in the Arctic vortex during AT-2, consistent with previous studies. In the SH middle stratosphere during AT-3, EqL/θ O_3 fields in middle EqLs depart from expectations. This departure is due to the fact that many of the ATMOS observations at low PV were taken in a low ozone pocket, which forms when low-latitude, high-O_3 air is drawn into and confined in the anticyclone for a number of days, where O_3 mixing ratios relax to much lower values. Photochemical mechanisms that depend primarily on solar conditions unrelated to vortex shape must thus be considered when analyzing maps of chemically active species in EqL/θ coordinates.

During fall, the largest differences in the tracer fields between the three ATLAS missions stem from the fact that each succeeding mission took place approximately 2 weeks later in the season. Both EqL tracer fields and calculations indicated progressively greater average descent of the air in the proto-vortex region for AT-1 (25 Mar–2 Apr 1992), AT-2, and AT-3. The differences in average descent result from both larger radiative cooling rates in the later missions, and greater confinement (which led to less mixing of air that had descended strongly with air that experienced weaker descent). The calculations also indicate greater isolation of air in the proto-vortex in later missions. During both AT-3 and AT-1, air that originated in the tropics in the month preceding the mission was sampled in the proto-vortex edge region, consistent with large tongues of low-latitude air being drawn up around the proto-vortex; whereas during AT-1 some of this air experienced net ascent in the previous month, during AT-3 all of the air originally from the tropics experienced net descent, confirming greater downward motion prior to AT-3. During AT-2, the proto-vortex was more quiescent, and ATMOS did not sample tropical air in the proto-vortex edge region.

The EqL/θ mapping of ATMOS observations from the three ATLAS missions has provided a detailed view of transport in and around the spring polar vortices and the developing vortices in fall. These fields are useful for other studies. They provide a common coordinate system for comparison of ATMOS observations with those from instruments that have simultaneous observations but different sampling patterns. Although the ATMOS observations do not provide complete global EqL coverage, the coverage is sufficient that these fields can also be used for some model initializations. Ongoing studies using the EqL/θ-mapped ATMOS data for these purposes will provide additional insight into the processes shaping trace gas fields in the spring and fall stratosphere.

Acknowledgments. We thank the ATMOS, CLAES, and MLS instrument teams for their role in producing those datasets, and the UKMO (R. Swinbank and A. O'Neill) for meteorological data. Work at the Jet Propulsion Laboratory, California Institute of Technology and the Lockheed Martin Advanced Technology Center was done under contract with the National Aeronautics and Space Administration. HAM was supported by the NASA Atmospheric Chemistry, Modeling, and Analysis Program (NAS1-98118).

References

Abbas, M. M., et al., Seasonal variations of water vapor in the lower stratosphere inferred from ATMOS/ATLAS-3 measurements of H_2O and CH_4, *Geophys. Res. Lett.*, *23*, 2401–2404, 1996.

Abrams, M. C., et al., ATMOS/ATLAS–3 observations of long-lived tracers and descent in the Antarctic vortex in November 1994, *Geophys. Res. Lett.*, *23*, 2341–2344, 1996a.

Abrams, M. C., et al., On the assessment and uncertainty of atmospheric trace gas burden measurements with high resolution infrared solar occultation spectra from space by the ATMOS experiment, *Geophys. Res. Lett.*, *23*, 2337–2340, 1996b.

Abrams, M. C., et al., Trace gas transport in the Arctic vortex inferred from ATMOS ATLAS–2 observations during April 1993, *Geophys. Res. Lett.*, *23*, 2345–2348, 1996c.

Allen, D. R., J. L. Stanford, M. A. López-Valverde, N. Nakamura, D. J. Lary, A. R. Douglass, M. C. Cerniglia, J. J. Remedios, and F. W. Taylor, Observations of middle atmosphere CO from the UARS ISAMS during the early northern winter 1991/1992, *J. Atmos. Sci.*, *56*, 563–583, 1999.

Austin, J., R. R. Garcia, J. M. Russell, III, S. Solomon, and A. F. Tuck, On the atmospheric photochemistry of nitric acid, *J. Geophys. Res.*, *91*, 5477–5485, 1986.

Bowman, K. P., Large-scale isentropic mixing properties of the Antarctic polar vortex from analyzed winds, *J. Geophys. Res.*, *98*, 23,013–23,027, 1993.

Brasseur, G., and S. Solomon, *Aeronomy of the Middle Atmosphere*. D. Reidel Publishing Company, Dordrecht, The Netherlands, second edn., 1986.

Butchart, N., and E. E. Remsberg, The area of the stratospheric polar vortex as a diagnostic for tracer transport on an isentropic surface, *J. Atmos. Sci.*, *43*, 1319–1339, 1986.

Callis, L. B., D. N. Baker, M. Natarajan, J. B. Blake, R. A. Mewaldt, R. S. Selesnick, and J. R. Cummings, A 2-D model simulation of downward transport of NO_y into the stratosphere: Effects on the 1994 austral spring O_3 and NO_y, *Geophys. Res. Lett.*, *23*, 1905–1908, 1996.

Dahlberg, S. P., and K. P. Bowman, Isentropic mixing in the Arctic stratosphere during the 1992–1993 and 1993–1994 winters, *Geophys. Res. Lett.*, *22*, 1237–1240, 1995.

Dunkerton, T. J., and D. P. Delisi, Evolution of potential vorticity in the winter stratosphere of January-February 1979, *J. Geophys. Res.*, *91*, 1199–1208, 1986.

Evans, S. J., R. Toumi, J. E. Harries, M. P. Chipperfield, and J. M. Russell, III, Trends in stratospheric humidity and the sensitivity of ozone to these trends, *J. Geophys. Res.*, *103*, 8715–8725, 1998.

Fahey, D. H., S. Solomon, S. R. Kawa, M. Loewenstein, J. R. Podolske, S. E. Strahan, and K. R. Chan, A diagnostic for denitrification in the winter polar stratospheres, *Nature*, *345*, 698–702, 1990a.

Fahey, D. H., K. K. Kelly, S. R. Kawa, A. F. Tuck, M. Loewenstein, K. R. Chan, and L. E. Heidt, Observations of denitrification and dehydration in the winter polar stratospheres, *Nature*, *344*, 321–324, 1990b.

Fisher, M., A. O'Neill, and R. Sutton, Rapid descent of mesospheric air into the stratospheric polar vortex, *Geophys. Res. Lett.*, *20*, 1267–1270, 1993.

Froidevaux, L., et al., Validation of the UARS Microwave Limb Sounder ozone measurements, *J. Geophys. Res.*, *101*, 10,017–10,060, 1996.

Gunson, M. R., et al., The Atmospheric Trace Molecule Spectroscopy (ATMOS) experiment: Deployment on the ATLAS Space Shuttle missions, *Geophys. Res. Lett.*, *23*, 2333–2336, 1996.

Hintsa, E. J., et al., Dehydration and denitrification in the arctic polar vortex during the 1995-1996 winter, *Geophys. Res. Lett.*, *25*, 501–504, 1998.

Jones, R. L., J. A. Pyle, J. E. Harries, A. M. Zavody, J. M. Russell, and J. C. Gille, The water vapour budget of the stratosphere studied using LIMS and SAMS satellite data, *Q. J. Roy. Meteor. Soc.*, *112*, 1127–1143, 1986.

Juckes, M. N., and A. O'Neill, Early winter in the northern hemisphere, *Q. J. Roy. Meteor. Soc.*, *114*, 1111–1125, 1988.

Koike, M., N. B. Jones, W. A. Matthews, P. V. Johnston, R. L. McKenzie, D. Kinnison, and J. Rodriguez, Impact of Pinatubo aerosols on the partitioning between NO_2 and HNO_3, *Geophys. Res. Lett.*, *21*, 597–600, 1994.

Kondo, Y., et al., NO_y-N_2O correlation observed inside the Arctic vortex in February 1997: Dynamical and chemical effects, *J. Geophys. Res.*, in press, 1999.

Kumer, J. B., et al., Comparison of correlative data with HNO_3 version 7 from the CLAES instrument deployed on the NASA Upper Atmosphere Research Satellite, *J. Geophys. Res.*, *101*, 9621–9656, 1996.

Lary, D. J., M. P. Chipperfield, J. A. Pyle, W. A. Norton, and L. P. Riishojgaard, Three-dimensional tracer initialization and general diagnostics using equivalent PV latitude-potential-temperature coordinates, *Q. J. Roy. Meteor. Soc.*, *121*, 187–210, 1995.

Manney, G. L., and R. W. Zurek, Interhemispheric comparison of the development of the stratospheric polar vortex during fall: A 3-dimensional perspective for 1991–92, *Geophys. Res. Lett.*, *20*, 1275–1278, 1993.

Manney, G. L., R. W. Zurek, M. E. Gelman, A. J. Miller, and R. Nagatani, The anomalous Arctic lower stratospheric polar vortex of 1992–1993, *Geophys. Res. Lett.*, *21*, 2405–2408, 1994a.

Manney, G. L., et al., Chemical depletion of ozone in the Arctic lower stratosphere during winter 1992-93, *Nature*, *370*, 429–434, 1994b.

Manney, G. L., R. W. Zurek, A. O'Neill, and R. Swinbank, On the motion of air through the stratospheric polar vortex, *J. Atmos. Sci.*, *51*, 2973–2994, 1994c.

Manney, G. L., L. Froidevaux, J. W. Waters, and R. W. Zurek, Evolution of Microwave Limb Sounder ozone and the polar vortex during winter, *J. Geophys. Res.*, *100*, 2953–2972, 1995a.

Manney, G. L., et al., Formation of low ozone pockets in the middle stratospheric anticyclone during winter, *J. Geophys. Res.*, *100*, 13,939–13,950, 1995b.

Manney, G. L., R. W. Zurek, L. Froidevaux, J. W. Waters, A. O'Neill, and R. Swinbank, Lagrangian transport calculations using UARS data. Part II: Ozone, *J. Atmos. Sci.*, *52*, 3069–3081, 1995c.

Manney, G. L., M. L. Santee, L. Froidevaux, J. W. Waters, , and R. W. Zurek, Polar vortex conditions during the 1995–96 Arctic winter: meteorology and MLS ozone, *Geophys. Res. Lett.*, *23*, 3203–3206, 1996a.

Manney, G. L., R. Swinbank, and A. O'Neill, Stratospheric meteorological conditions for the 3–12 Nov 1994 ATMOS/ATLAS–3 measurements, *Geophys. Res. Lett.*, *23*, 2409–2412, 1996b.

Manney, G. L., L. Froidevaux, M. L. Santee, R. W. Zurek, and J. W. Waters, MLS observations of Arctic ozone loss in 1996–97, *Geophys. Res. Lett.*, *24*, 2697–2700, 1997.

Manney, G. L., J. C. Bird, D. P. Donovan, T. J. Duck, J. A. Whiteway, S. R. Pal, and A. I. Carswell, Modeling ozone laminae in ground-based Arctic wintertime observations using trajectory calculations and satellite data, *J. Geophys. Res.*, *103*, 5797–5814, 1998.

Michelsen, H. A., et al., Intercomparison of ATMOS, SAGE II, and ER-2 observations in Arctic vortex and extra-vortex air masses during spring 1993, *Geophys. Res. Lett.*, *26*, 291–294, 1999.

Michelsen, H. A., G. L. Manney, M. R. Gunson, C. P. Rinsland, and R. Zander, Correlations of stratospheric abundances of CH_4 and N_2O derived from ATMOS measurements, *Geophys. Res. Lett.*, *25*, 2777–2780, 1998a.

Michelsen, H. A., G. L. Manney, M. R. Gunson, and R. Zander, Correlations of stratospheric abundances of NO_y, O_3, N_2O, and CH_4 derived from ATMOS measurements, *J. Geophys. Res.*, *103*, 28,347–28,359, 1998b.

Morrey, M. W., and R. S. Harwood, Interhemispheric differences in stratospheric water vapour during late winter, in version 4 MLS measurements, *Geophys. Res. Lett.*, *25*, 147–150, 1998.

Morris, G. A., et al., Trajectory mapping and applications to data from the Upper Atmosphere Research Satellite, *J. Geophys. Res.*, *100*, 16,491–16,505, 1995.

Morris, G. A., S. R. Kawa, A. R. Douglass, M. R. Schoeberl, L. Froidevaux, and J. W. Waters, Low ozone pockets explained, *J. Geophys. Res.*, *103*, 3599–3610, 1998.

Mote, P. W., et al., An atmospheric tape recorder: The imprint of tropical tropopause temperatures on stratospheric water vapor, *J. Geophys. Res.*, *101*, 3989–4006, 1996.

Nair, H., M. Allen, L. Froidevaux, and R. W. Zurek, Localized rapid ozone loss in the northern winter stratosphere: An analysis of UARS observations, *J. Geophys. Res.*, *103*, 1555–1571, 1998.

Nedoluha, G. E., D. E. Siskind, J. T. Bacmeister, R. M. Bevilacqua, and J. M. Russell, III, Changes in upper stratospheric CH_4 and NO_2 as measured by HALOE and implications for changes in transport, *Geophys. Res. Lett.*, *25*, 987–990, 1998a.

Nedoluha, G. E., R. M. Bevilacqua, R. M. Gomez, D. E. Siskind, B. C. Hicks, J. M. Russell, III, and B. J. Connor, Increases in middle atmospheric water vapor as observed by the Halogen Occultation Experiment and the ground-based Water Vapor Millimeter-wave Spectrometer from 1991 to 1997, *J. Geophys. Res.*, *103*, 3531–3543, 1998b.

Newman, P. A., et al., Measurements of polar vortex air in midlatitudes, *J. Geophys. Res.*, *101*, 12,879–12,891, 1996.

Oltmans, S. J., and D. J. Hofmann, Increase in lower-stratospheric water vapor at a mid-latitude northern hemisphere site from 1981 to 1994, *Nature*, *374*, 146–149, 1995.

O'Neill, A., and V. D. Pope, The seasonal evolution of the extra-tropical stratosphere in the southern and northern hemispheres: Systematic changes in potential vorticity and the non-conservative effects of radiation, in *Dynamics, Transport and Photochemistry in the Middle Atmosphere of the Southern Hemisphere*, edited by A. O'Neill, pp. 33–54. Kluwer Academic Publishers, Dordrecht, The Netherlands, 1990.

Plumb, R. A., D. W. Waugh, R. J. Atkinson, P. A. Newman, L. R. Lait, M. R. Schoeberl, E. V. Browell, A. J. Simmons, and M. Loewenstein, Intrusions into the lower stratospheric Arctic vortex during the winter of 1991–1992, *J. Geophys. Res.*, *99*, 1089–1105, 1994.

Pumphrey, H. C., Nonlinear retrievals of water vapour from the UARS Microwave Limb Sounder (MLS), *Adv. Sp. Res.*, *21*, 389–392, 1998.

Randel, W. J., and F. Wu, Climatology of stratospheric ozone based on SBUV and SBUV/2 data: 1978–1994, Tech. Rep. NCAR/TN-412+STR, National Center for Atmospheric Research, 1995.

Randel, W. J., F. Wu, J. M. Russell, III, A. E. Roche, and J. W. Waters, Seasonal cycles and QBO variations in stratospheric CH_4 and H_2O observed in UARS HALOE data, *J. Atmos. Sci.*, *55*, 163–185, 1998.

Randel, W. J., F. Wu, J. M. Russell, III, and J. W. Waters, Space-time patterns of trends in stratospheric constituents derived from UARS measurements, *J. Geophys. Res.*, in press, 1999.

Rinsland, C. P., et al., ATMOS measurements of $H_2O + 2CH_4$ and total and total reactive nitrogen in the November 1994 Antarctic stratosphere: Dehydration and denitrification in the vortex, *Geophys. Res. Lett.*, *23*, 2397–2400, 1996a.

Rinsland, C. P., et al., ATMOS/ATLAS–3 measurements of stratospheric chlorine and reactive nitrogen partitioning inside and outside the November 1994 Antarctic vortex, *Geophys. Res. Lett.*, *23*, 2365–2368, 1996b.

Rinsland, C. P., M. R. Gunson, M. C. Abrams, L. L. Lowes, R. Zander, E. Mahieu, A. Goldman, and F. W. Irion, April 1993 Arctic profiles of stratospheric HCl, $ClONO_2$, and CCl_2F_2 from atmospheric trace molecule spectroscopy/ATLAS 2 infrared solar occultation spectra, *J. Geophys. Res.*, *100*, 14,019–14,027, 1995.

Rinsland, C. P., et al., Polar stratospheric descent of NO_y and CO and Arctic denitrification during winter 1992–93, *J. Geophys. Res.*, *104*, 1847–1861, 1999.

Roche, A. E., et al., Validation of CH_4 and N_2O measurements by the Cryogenic Limb Array Etalon Spectrometer instrument on the Upper Atmosphere Research Satellite, *J. Geophys. Res.*, *101*, 9679–9710, 1996.

Ruth, S., R. Kennaugh, L. J. Gray, and J. M. Russell, III, Seasonal, semiannual, and interannual variability seen in measurements of methane made by the UARS Halogen Occultation Experiment, *J. Geophys. Res.*, *102*, 16,189–16,199, 1997.

Santee, M. L., G. L. Manney, L. Froidevaux, W. G. Read, and J. W. Waters, Six years of UARS Microwave Limb Sounder HNO_3 observations: Seasonal, interhemispheric, and interannual variations in the lower stratosphere, *J. Geophys. Res.*, in press, 1999.

Schoeberl, M. R., et al., Reconstruction of the constituent distribution and trends in the Antarctic polar vortex from ER-2 flight observations, *J. Geophys. Res.*, *94*, 16,815–16,845, 1989.

Schoeberl, M. R., L. R. Lait, P. A. Newman, and J. E. Rosenfield, The structure of the polar vortex, *J. Geophys. Res.*, *97*, 7859–7882, 1992.

Schoeberl, M. R., M. Luo, and J. E. Rosenfield, An analysis of the Antarctic Halogen Occultation Experiment trace gas observations, *J. Geophys. Res.*, *100*, 5159–5172, 1995.

Strahan, S. E., J. E. Nielson, and M. C. Cerniglia, Long-lived tracer transport in the Antarctic stratosphere, *J. Geophys. Res.*, *101*, 26,615–26,629, 1996.

Sugita, T., et al., Denitrification observed inside the Arctic vortex in February 1995, *J. Geophys. Res.*, *103*, 16,221–16,233, 1998.

Sutton, R. T., H. MacLean, R. Swinbank, A. O'Neill, and F. W. Taylor, High-resolution stratospheric tracer fields estimated from satellite observations using lagrangian trajectory calculations, *J. Atmos. Sci.*, *51*, 2995–3005, 1994.

Swinbank, R., and A. O'Neill, A stratosphere-troposphere data assimilation system, *Mon. Wea. Rev.*, *122*, 686–702, 1994.

Vömel, H., M. Rummukainen, R. Kivi, J. Karhu, T. Turunen, E. Kyrö, J. Rosen, N. Kjome, and S. Oltmans, Dehydration and sedimentation of ice particles in the Arctic stratospheric vortex, *Geophys. Res. Lett.*, *24*, 795–798, 1997.

Waugh, D. W., et al., Mixing of polar vortex air into middle latitudes as revealed by tracer-tracer scatterplots, *J. Geophys. Res.*, *102*, 13,119–13,134, 1997.

Waugh, D. W., and W. J. Randel, Climatology of Arctic and Antarctic polar vortices using elliptical diagnostics, *J. Atmos. Sci.*, in press, 1999.

Zurek, R. W., G. L. Manney, A. J. Miller, M. E. Gelman, and R. M. Nagatani, Interannual variability of the north polar vortex in the lower stratosphere during the UARS mission, *Geophys. Res. Lett.*, *23*, 289–292, 1996.

G. L. Manney (M/S 183-701, manney@mls.jpl.nasa.gov), M. R. Gunson (M/S 169-237), F. W. Irion (M/S 183-601), N. J. Livesey (M/S 183-701), M. L. Santee (M/S 183-701), Jet Propulsion Laboratory, Pasadena, CA 91109.

H. A. Michelsen, Atmospheric and Environmental Research, Inc., 2682 Bishop Dr., Ste 120, San Ramon, CA 94583

A. E. Roche, Lockheed Martin Advanced Technology Center, Org H1-11, Bldg 255, 3251 Hanover St., Palo Alto, CA 94304

This preprint was prepared with AGU's LaTeX macros v4, with the extension package 'AGU++' by P. W. Daly, version 1.5d from 1997/04/28.